Chaperone requirements for de novo folding of *Saccharomyces cerevisiae* septins

Daniel Hassell, Ashley Denney, Emily Singer, Aleyna Benson, Andrew Roth, Julia Ceglowski, Marc Steingesser, and Michael McMurray*
University of Colorado Anschutz Medical Campus, Aurora, CO 80045

ABSTRACT **Polymers of septin protein complexes play cytoskeletal roles in eukaryotic cells. The specific subunit composition within complexes controls functions and higher-order structural properties. All septins have globular GTPase domains. The other eukaryotic cytoskeletal NTPases strictly require assistance from molecular chaperones of the cytosol, particularly the cage-like chaperonins, to fold into oligomerization-competent conformations. We previously identified cytosolic chaperones that bind septins and influence the oligomerization ability of septins carrying mutations linked to human disease, but it was unknown to what extent wild-type septins require chaperone assistance for their native folding. Here we use a combination of in vivo and in vitro approaches to demonstrate chaperone requirements for de novo folding and complex assembly by budding yeast septins. Individually purified septins adopted nonnative conformations and formed nonnative homodimers. In chaperonin- or Hsp70-deficient cells, septins folded slower and were unable to assemble posttranslationally into native complexes. One septin, Cdc12, was so dependent on cotranslational chaperonin assistance that translation failed without it. Our findings point to distinct translation elongation rates for different septins as a possible mechanism to direct a stepwise, cotranslational assembly pathway in which general cytosolic chaperones act as key intermediaries.**

Monitoring Editor
Amy Gladfelter
University of North Carolina, Chapel Hill

Received: Jul 11, 2022
Accepted: Aug 2, 2022

INTRODUCTION

Septins evolved from ancient GTPases into a diverse family of eukaryotic proteins capable of assembling into hetero-oligomers (Shuman and Momany, 2021). Septin hetero-oligomers further polymerize into cytoskeletal filaments involved in a variety of cellular functions (Woods and Gladfelter, 2021). In many cell types no septin monomer can be found (Frazier *et al.*, 1998; Bridges *et al.*, 2014; Abbey *et al.*, 2016). Similarly, the building blocks of microtubules are stable heterodimers of α- and β-tubulins, and individual tubulin proteins exist fleetingly, in complexes with cytosolic chaperones and dedicated folding cofactors (Lewis *et al.*, 1997). The human septin mutation SEPT12(Asp197Asn) causes disease by interfering with filament assembly (Kuo *et al.*, 2012) but was first identified 40 years prior in the homologous septin in the budding yeast *Saccharomyces cerevisiae*, as Cdc10(Asp182Asn) (Hartwell, 1971; McMurray *et al.*, 2011b). We found that this mutation slows folding of the yeast septin and prolongs interactions with cytosolic chaperones, leading to a kinetic delay in the ability of the mutant septin to stably incorporate into functional septin hetero-oligomers (Johnson *et al.*, 2015; Denney *et al.*, 2021). Our other studies provided evidence that conformational changes at septin-septin interfaces—some linked to GTP binding and/or hydrolysis—are important for an efficient, step-wise pathway of de novo septin hetero-oligomer assembly (Weems *et al.*, 2014; Weems and McMurray, 2017; Johnson *et al.*, 2015). These findings support a model in which a newly translated septin can explore a variety of conformations, at least some of which bind cytosolic chaperones, before achieving its native conformation in the context of a septin hetero-oligomer. It was unclear to what extent chaperone function promotes wild-type septin folding and hetero-oligomerization.

Chaperonins are large, oligomeric chaperones that form a client-binding chamber and couple the hydrolysis of ATP

This article was published online ahead of print in MBoC in Press (http://www.molbiolcell.org/cgi/doi/10.1091/mbc.E22-07-0262) on August 10, 2022.

Conflict of interest: The authors declare that they have no conflict of interest.

*Address correspondence to: Michael McMurray (michael.mcmurray@cuanschutz.edu).

Abbreviations used: CCT, chaperonin containing TCP1; SEC, size exclusion chromatography.

to conformational changes that promote client folding and eventual release (Hayer-Hartl *et al.*, 2016; Gestaut *et al.*, 2019). Chaperonins diverged during evolution into two groups. A proteomics study querying the proteins bound by the group II chaperonin of the *S. cerevisiae* cytosol—called chaperonin containing tailless complex polypeptide 1 (CCT) or tailless complex polypeptide 1 ring complex (TRiC)—and released upon ATP hydrolysis identified Cdc3, Cdc10, Cdc11, Cdc12, and Shs1, the five septin proteins that are expressed in mitotically dividing cells (Dekker *et al.*, 2008). An independent study also found copurification with CCT of an overexpressed, GST-tagged yeast septin, Cdc10 (Yam *et al.*, 2008). A more recent study specifically investigating cotranslational CCT interactions identified ribosomes translating yeast septins (Stein *et al.*, 2019). Finally, our split-protein complementation assay studies demonstrated in living yeast cells that multiple CCT subunits interact with multiple septins (Denney *et al.*, 2021). Thus all available evidence supports direct interactions between nascent yeast septins and CCT. However, chaperone binding does not necessarily mean that the chaperone plays a functional role in de novo folding. Indeed, a role for CCT–septin interactions in promoting efficient de novo septin folding was previously dismissed (Dekker *et al.*, 2008), for two reasons. First, septins successfully fold and hetero-oligomerize when heterologously expressed in *Escherichia coli* (Versele and Thorner, 2004; Versele *et al.*, 2004; Farkasovsky *et al.*, 2005; Bertin *et al.*, 2008), which lacks CCT and instead has a group I chaperonin, GroEL. Second, yeast Cdc10 synthesized by *E. coli* ribosomes in a cell-free translation reaction migrates in native PAGE in a way that is unaffected by the addition of purified CCT (Dekker *et al.*, 2008), suggesting that CCT does not influence Cdc10 conformation. Those authors concluded that "it is unlikely that CCT is required to fold septins *de novo*" and "septins probably do not need CCT for biogenesis or folding" (Dekker *et al.*, 2008). Here we experimentally address chaperone roles in de novo septin folding.

By "shielding" exposed regions normally buried in the core of a folded protein or in a protein–protein interface, chaperone binding helps client proteins avoid making inappropriate inter- and intramolecular interactions and becoming "trapped" in low-energy, nonnative conformations (Balchin *et al.*, 2016). Septin–septin interactions in the context of native septin oligomers presumably also help the individual proteins maintain native conformations and avoid inappropriate interactions. Indeed, a purified single human septin is prone to amyloid aggregation under conditions where a septin heterodimer is not, suggesting that native septin oligomerization prevents amyloid formation (Kumagai *et al.*, 2019). Similarly, early studies of septin subunit organization within hetero-oligomers were misled by nonnative interactions found when individual septins were expressed individually in *E. coli* and purified away from all other proteins (including chaperones) before mixing with other individually expressed and purified septins (Versele *et al.*, 2004). For example, purified Cdc12 interacted robustly with Cdc10 and with itself (Versele *et al.*, 2004), but neither of these interactions occurs within native hetero-oligomers, which are linear octamers with subunit order Cdc11–Cdc12–Cdc3–Cdc10–Cdc10–Cdc3–Cdc12–Cdc11 (Bertin *et al.*, 2008) or Shs1–Cdc12–Cdc3–Cdc10–Cdc10–Cdc3–Cdc12–Cdc11 (Garcia *et al.*, 2011). Here we used genetic, biochemical, and biophysical methods to obtain new insights into the conformations of "isolated" septins, their ability to assemble into native hetero-oligomers, and roles for cytosolic chaperones in maintaining that ability.

RESULTS

Slower septin folding/assembly in chaperone-mutant yeast cells

To ask whether chaperone function is required for efficient de novo septin folding in living cells, we used a plasmid in which transcription of C-terminally GFP-tagged Cdc3 is under control of the galactose-inducible *GAL1/10* promoter and quantified the kinetics of fluorescence accumulation following the addition of galactose to the growth medium (Figure 1A). Localization to rings of septin filaments at yeast bud necks was taken as evidence that Cdc3-GFP folded properly and coassembled with endogenous untagged septins into native hetero-oligomers. We interpreted fluorescence away from bud necks (in the cytoplasm/nucleus) as a composite of unpolymerized septin hetero-oligomers containing Cdc3-GFP plus "excess" or misfolded Cdc3-GFP monomers. In wild-type cells, very few septin monomers can be found by either biochemical (Frazier *et al.*, 1998) or microscopy-based (Bridges *et al.*, 2014) approaches, indicating that septin folding and higher-order assembly are normally very efficient. Accordingly, in our experimental setup we suspect that transcription and translation are normally the rate-limiting steps for accumulation of fluorescent signal in septin rings. We previously used the same assay to find evidence that a mutation (Gly365Arg) in the "G" dimerization interface—which encompasses the GTP-binding pocket—slows folding of the mutant Cdc3 to the point that we can detect a delay in the accumulation of septin ring fluorescence over time (Schaefer *et al.*, 2016). Here, we kept Cdc3 wild type and instead mutated cytosolic chaperones.

We tested CCT using *cct4-1*, in which the Cct4 subunit carries a Gly345Asp substitution that interferes with cooperativity of ATP binding between the two rings of the chaperonin complex (Shimon *et al.*, 2008). Cdc3-GFP mislocalization as misshapen septin rings and aberrant cortical patches was previously seen in the same *cct4* mutant at the restrictive temperature of 37°C, where septins no longer copurify with the mutant CCT (Dekker *et al.*, 2008). At 37°C the mutant cells also make multiple, elongated buds (Shimon *et al.*, 2008), hallmarks of septin dysfunction. Our assay for septin folding kinetics requires that the mutant cells proliferate at the same rate as wild-type cells; otherwise differences in fluorescence could be attributed to changes in dilution through cell divisions. Hence we cultured the cells at room temperature (22°C; see Figure 3B later in this article). We suspected that CCT–septin interactions would be compromised in *cct4-1* cells even at permissive temperatures because 1) the actin-folding activity in vitro of purified CCT carrying mutant Cct4(Gly354Asp) subunits is crippled to the same extent at permissive and restrictive temperatures (Shimon *et al.*, 2008); and 2) at an otherwise permissive temperature *cct4-1* displays a negative genetic interactions when combined with another slow-folding G-interface mutant septin, Cdc10(Asp182Asn) (Johnson *et al.*, 2015; Costanzo *et al.*, 2016). Indeed, the temperature-sensitive nature of the *cct4* mutant may say more about the adverse effects of high temperatures on wild-type protein folding than on Cct4(Gly354Asp) function per se.

The accumulation of fluorescent Cdc3-GFP signal in septin rings was delayed in *cct4* mutants relative to wild-type cells, with almost no increase in the mutant cells between the 3.5- and 5.5-h time points postinduction, but by 6.5 h septin rings were as bright as in wild-type cells (Figure 1B). Cytoplasmic/nuclear signal also lagged in *cct4* cells but eventually exceeded wild-type levels (Figure 1B). These data may point to less efficient septin translation in chaperone-mutant cells. Indeed, inhibition of human chaperones slows translational elongation of many proteins, which has been proposed to reflect loss of a cotranslational "pulling force" that the chaperones

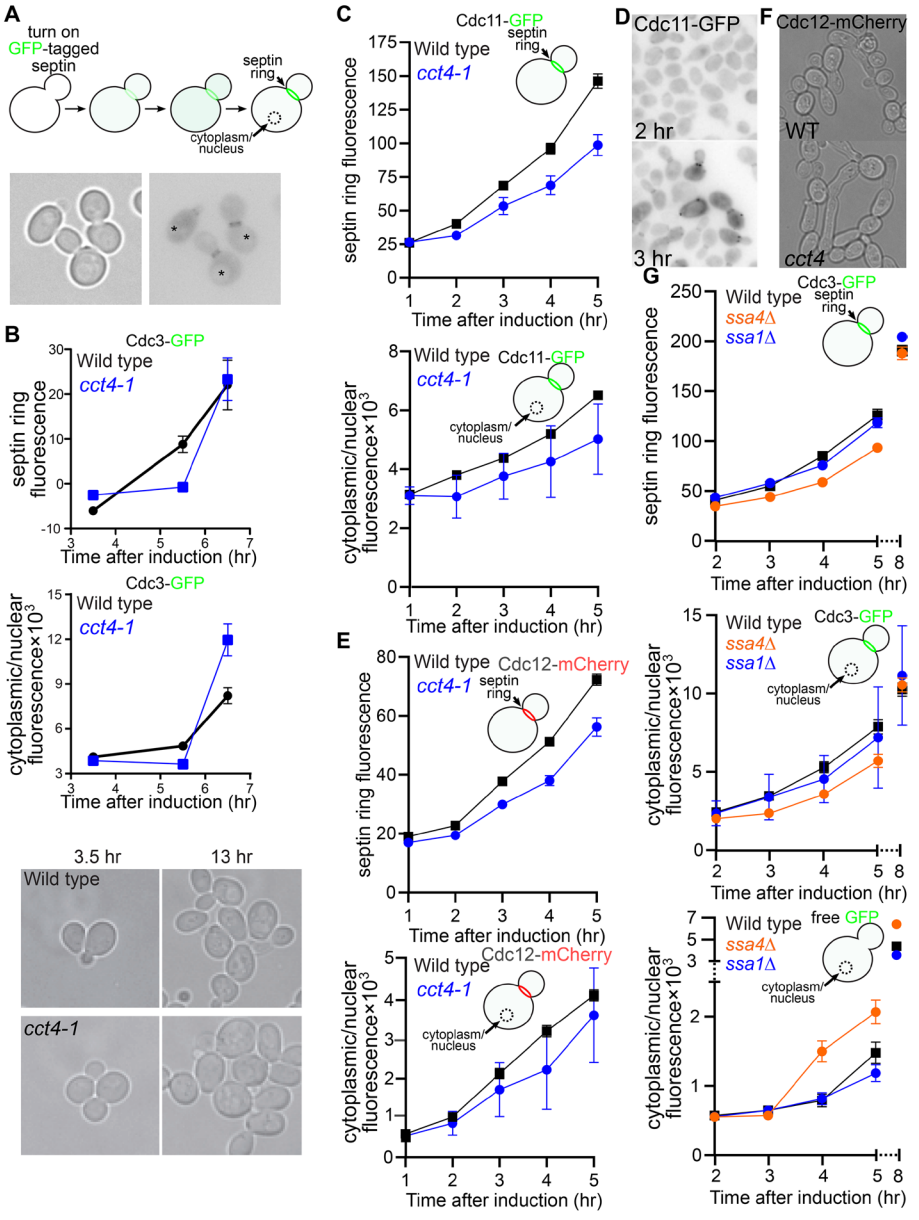

FIGURE 1: Chaperone requirements for efficient de novo septin folding. (A) Schematic illustration of experimental approach. Localization to septin filaments in septin rings at bud necks or in the cytoplasm/nucleus is monitored at time points following the induction of new synthesis of a GFP-tagged septin under control of the galactose-inducible *GAL1/10* promoter. Signal is quantified at the bud neck or in a circular region of the cytoplasm/nucleus, avoiding the vacuole. Micrographs are representative cells from a middle time point in an actual experiment. Left panel, transmitted light; right panel, fluorescent signal shown as dark pixels on a light background. Asterisks are centered in presumptive vacuoles. (B) Wild-type cells (BY4741) or *cct4* mutant cells (CBY11211) carrying plasmid pMVB1 were grown in synthetic medium with 2% raffinose and loaded into a microfluidic chamber. Medium containing 1.95% raffinose and 0.05% galactose was introduced, and images were taken at the indicated time points thereafter. At least 46 cells were analyzed per genotype per time point. Points show means, error bars are SEM. The micrographs show the same fields of cells at two time points, demonstrating similar rates of cell division for the wild-type and mutant cells. (C, E) As in B but with Cdc11-GFP plasmid pMVB3 or Cdc12-mCherry plasmid pGF-IVL-470. Cells were grown in culture tubes, and aliquots were removed for imaging at the indicated time points. At least 22 cells were analyzed per genotype per time point. (D) Fluorescence micrographs for representative wild-type cells from the Cdc11-GFP experiment in C imaged after the indicated time postinduction. (F) Cells ("WT," BY4741; "*cct4*," CBY11211) with Cdc12-mCherry plasmid pGF-IVL-470 were cultured in selective medium containing 1.95% raffinose and 0.05% galactose for 24 h. At 11 h, cells were diluted to prevent culture saturation. (G) As in B but with strains H00504 ("*ssa1Δ*") and H00507 ("*ssa4Δ*") and, as indicated, Cdc3-GFP plasmid pMVB1 or GFP alone plasmid pTS395. At least 30 cells were analyzed per genotype per time point.

normally exert on a nascent client peptide emerging from the ribosome exit tunnel (Liu *et al.*, 2013; Shalgi *et al.*, 2013). Previous studies using analogous galactose-induction assays but testing a different client protein demonstrated that CCT function is dispensable for efficient transcriptional induction by the *GAL1/10* promoter (Kim *et al.*, 1998). GFP folds independently of chaperones (Weissman *et al.*, 1996; Makino *et al.*, 1997). Thus these data support a requirement for CCT function in efficient de novo septin folding.

We examined two other septins in *cct4* mutants and found equivalent overall results, with some noteworthy differences (Figure 1, C–F). Above a threshold level of expression, in addition to the cytoplasmic/nuclear and bud neck localization patterns, some Cdc11-GFP localized to cortical foci (Figure 1D). To our knowledge, such foci have not been previously reported. Unlike Cdc3, Cdc10, or Cdc12, high Cdc11 levels are known to perturb septin ring assembly/function (Sopko *et al.*, 2006), presumably by "capping" the ends of hetero-octamers with extra Cdc11 molecules and thereby inhibiting filament polymerization (Takagi *et al.*, 2021). These foci may thus represent clusters of septin complexes able to interact with the membrane but unable to polymerize properly. Regardless of the underlying mechanism, the foci were not solely responsible for the observed differences in kinetics for *cct4* cells, because differences were apparent at time points before foci appeared (Figure 1, C and D). The Cdc11-GFP foci interfered with reliable septin ring signal quantification at late time points, however, so we ended the experiment before being able to ask whether Cdc11-GFP incorporation eventually "caught up" in the *cct4* cells compared with wild type. We also were unable to see whether Cdc12-mCherry signal "caught up," because at high expression levels these cells became elongated; this defect was worse in *cct4* mutants (Figure 1F). Nonetheless, these data demonstrate that multiple septins require full chaperonin function for efficient assembly into polymerization-competent complexes.

Chaperonin assistance is necessary but not sufficient for the de novo folding of other cytoskeletal NTPases; other chaperones are also required (Gao *et al.*, 1993; Vainberg *et al.*, 1998; Machida *et al.*, 2021). Two paralogous ribosome-associated Hsp70 chaperones of the Stress Seventy B subfamily, Ssb1 and Ssb2, interact cotranslationally with more than half of all actively translated proteins, including Cdc3, Cdc10, Cdc11, and Cdc12 (Willmund *et al.*, 2013;

Stein *et al.*, 2019). All septins were found in aggregates in *ssb1*Δ *ssb2*Δ cells (Willmund *et al.*, 2013). Hence the Ssb chaperones were compelling candidates for our analysis. *ssb1*Δ *ssb2*Δ cells proliferate slowly at best (Nelson *et al.*, 1992), precluding analysis with our kinetic assay, but multiple phenotypes have been observed in *ssb1*Δ *SSB2*$^{+}$ cells (Dunn and Jensen, 2003; Alamgir *et al.*, 2010; Naicker *et al.*, 2012). We had also noticed a septin phenotype: an increase in apparent aggregates (cytoplasmic foci) when we overexpressed Cdc10(Asp182Asn)-GFP and cultured cells at 37°C (Supplemental Figure 1A), pointing to a possible defect in septin folding in the absence of only Ssb1. However, when we measured the kinetics of septin ring signal accumulation in *ssb1*Δ cells following induction of expression of plasmid-encoded Cdc12-mCherry, we saw no difference compared with wild type (Supplemental Figure 1B).

We previously found interactions between septins and other partly redundant members of the yeast cytosolic Hsp70 chaperone family, including the Stress Seventy subfamily A chaperones Ssa2, Ssa3, and Ssa4 but not Ssa1 (Denney *et al.*, 2021), which is 98% identical to Ssa2. We tested *ssa1*Δ and *ssa4*Δ mutants and found a delay in Cdc3-GFP fluorescence in septin rings in *ssa4*Δ cells but not in *ssa1*Δ cells (Figure 1G). The delay in Cdc3-GFP accumulation in *ssa4*Δ cells may have been partially masked by higher induction from the *GAL1/10* promoter at later time points, because in these cells free GFP expressed from an otherwise identical plasmid accumulated faster than in wild-type or *ssa1*Δ cells (Figure 1G).

Hsp90-family chaperones typically act downstream of Hsp70s in client folding (Morán Luengo *et al.*, 2019). *S. cerevisiae* has two paralogous cytosolic Hsp90 family members, Hsc82 and Hsp82, both of which we found to bind septins in vivo (Denney *et al.*, 2021). These genes are only partially redundant, because deletion of either one is sufficient to confer some phenotypes (e.g., freeze tolerance [Naicker *et al.*, 2012]) and to alter the phenotypes caused by mutations in other, nonchaperone genes, including *CDC10* (Costanzo *et al.*, 2010). We found no difference in Cdc3-GFP folding kinetics in cells lacking either Hsc82 or Hsp82 (Supplemental Figure 1C). An important caveat to our Ssb- and Hsp90-negative results is that because the range of effects detectable by our kinetic assay is rather narrow—chaperone mutations must not be so severe as to slow cell division or perturb septin ring morphology but severe enough to cause a phenotype—the failure to detect an effect cannot be interpreted as a lack of chaperone involvement in septin folding. Our data point to CCT and Ssa4 as important for efficient de novo septin folding.

Nonnative conformations and oligomerization by individual purified septins

If chaperones are important in promoting septin folding before septin–septin interaction during oligomerization, then individual septins might misfold in the absence of chaperones and partner septins. To explore in greater detail the ways that yeast septins fold and oligomerize in the absence of chaperones and other septins, we used a published plasmid (Versele and Thorner, 2004) to purify hexahistidine-tagged ("6xHis") Cdc3 following *E. coli* expression. In the original study, the oligomerization status of 6xHis-Cdc3 was not determined. It was capable of binding robustly to purified GST-Cdc12 or GST-Cdc10, the native interaction partners (Versele *et al.*, 2004), suggesting that at least some molecules had interfaces available for native interactions. We used a centrifugal filtration column with a nominal 100-kDa molecular weight cutoff and found that, like homotetrameric alcohol dehydrogenase (Adh1, native molecular weight ~150 kDa, monomer molecular weight 37 kDa), 6xHis-Cdc3 (monomeric molecular weight ~60 kDa) remained in the retentate fraction (Figure 2A), suggestive of homo-oligomerization. Consistent with all prior reports, Cdc3 migrated anomalously during SDS–PAGE, at an apparent molecular weight of ~70 kDa.

In analytical size exclusion chromatography (SEC), 6xHis-Cdc3 eluted as an ~1:1 mix of an apparent monomer and homodimer (Figure 2B). The monomer eluted later than 45-kDa ovalbumin (Figure 2B), suggestive of a nonspherical shape and/or interactions with the column media. The apparent dimer eluted as expected (~120 kDa). These results indicate that in the absence of native interaction partners (i.e., chaperones and other septins) Cdc3 is prone to nonnative homodimerization. Nonnative Cdc3 homodimerization via the G interface allows septin filament formation in the absence of Cdc10 (McMurray *et al.*, 2011a; Johnson *et al.*, 2020). Exogenous addition of GDP or a GTP analogue was able to drive G interface–mediated dimerization of a purified human septin (Sirajuddin *et al.*, 2007), and exogenous guanidine hydrochloride promotes nonnative Cdc3 homodimerization in vivo (Johnson *et al.*, 2020). We added an excess of GTP and/or guanidine hydrochloride at various concentrations and repeated the SEC analysis. Neither small molecule changed the Cdc3 monomer:dimer ratio (Figure 2C), suggesting that homodimerization did not occur via the G interface.

To gain further insights into the conformation of Cdc3 and the mechanism of homodimerization, we performed hydrogen-deuterium exchange mass spectrometry (HDX-MS) and mapped exchange ratios onto the Cdc3 amino acid sequence (Supplemental Figure 2) and the predicted structure of Cdc3 (Figure 2D). MS results confirmed that the purified protein was full length, though some internal peptides were not represented (~85% coverage; Figure 2D and Supplemental Figure 2). Consistent with the SEC results, every peptide in the HDX-MS data was flagged by the analysis software for likely "EX1" kinetics (poor fit to binomial distribution), pointing to a mixture of at least two distinct conformations.

Among the five septins expressed in mitotically dividing yeast cells, Cdc3 is unique in having an ~100-residue N-terminal extension (NTE), which exhibits a very high, evolutionarily conserved predicted propensity for intrinsic disorder (Weems and McMurray, 2017). We previously proposed that the Cdc3 NTE interacts weakly with the Cdc3 G interface to inhibit G dimerization with Cdc10 until Cdc3–Cdc12 interaction across the NC interface repositions the NTE and allows Cdc10 access (Weems and McMurray, 2017). Consistent with this model, the entire NTE exhibited high exchange ratios (Figure 2D and Supplemental Figure 2), suggestive of high solvent accessibility. (Note that the position of the NTE in the structural model in Figure 2D is a low-confidence prediction.)

Moving C-terminally along 6xHis-Cdc3, the exchange ratio abruptly decreased near the α0 helix (Figure 2D and Supplemental Figure 2), a key feature of the other septin dimerization interface, called "NC." Other portions of the NC interface, including the α5 helix, also exhibited slower exchange (Figure 2D and Supplemental Figure 2). We note that the sequences in many regions that exhibited less exchange are rich in hydrophobic amino acids. We interpret these data as evidence that Cdc3 purified in these conditions is at least partially folded, burying hydrophobic/aggregation-prone regions in intra- or intermolecular contacts, but is mostly in an unstable, largely nonnative conformation.

Regions normally buried in the G dimer interface showed relatively high exchange, including the G1 motif/P loop, the Sep4 motif/β7-β8 hairpin, the *trans* loop 1, and the G3 motif/Switch II loop (Supplemental Figure 2). The C-terminal extension, or CTE, displayed high exchange except for a region within the hydrophobic heptad repeats predicted to mediate formation of a coiled-coil (Versele *et al.*, 2004) (Figure 2D and Supplemental Figure 2). This

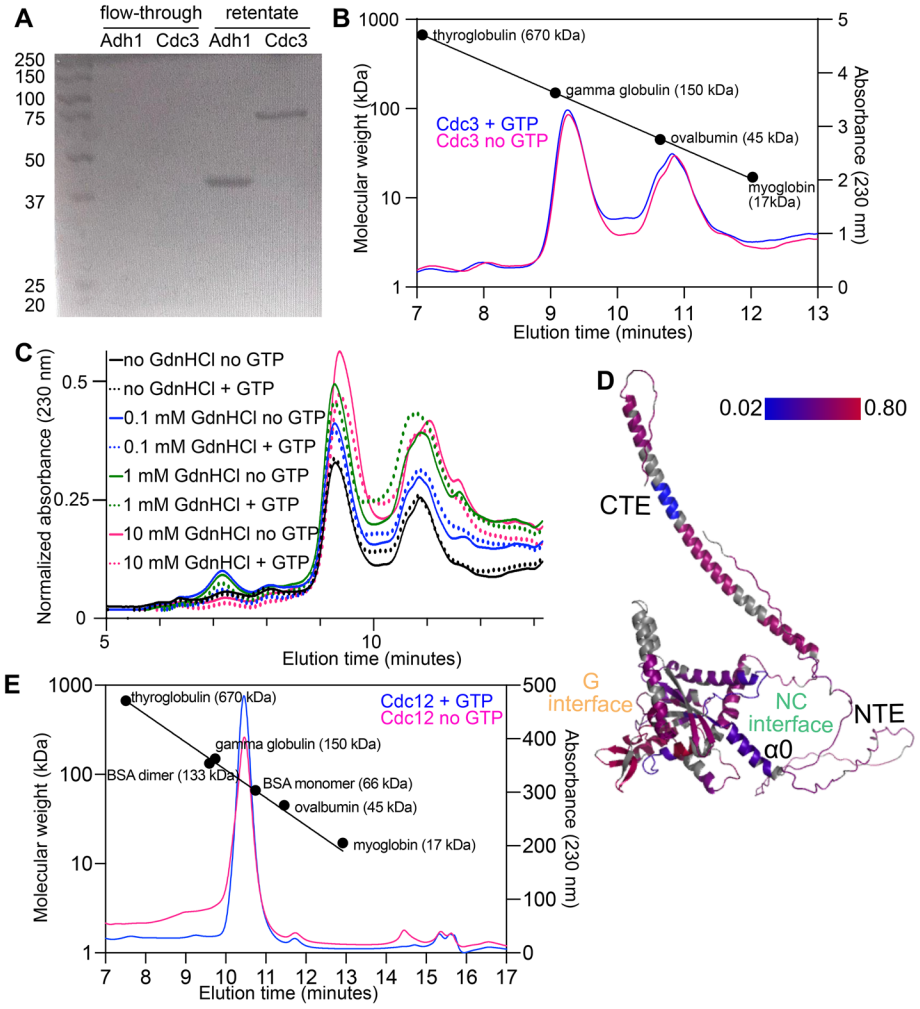

FIGURE 2: Nonnative homodimerization by purified yeast septins. (A) Purified tetrameric Adh1 (native molecular weight ~150 kDa) and purified 6xHis-Cdc3 (monomeric molecular weight ~60 kDa) were centrifuged through a 100-kDa-cutoff filtration device. Portions of the flow-through and retentate were separated by SDS–PAGE and stained with Coomassie. Leftmost lane contains molecular weight ladder (Thermo Fisher Scientific #SM0331). (B) Samples of molecular weight standards or 6xHis-Cdc3 were analyzed by size exclusion chromatography, and the 230-nm absorbance profiles, indicative of protein concentration, were plotted as a function of elution time. Colored lines show 6xHis-Cdc3 with or without added GTP. Circles show peak elution times for the indicated standards. (C) As in B, but only with samples of 6xHis-Cdc3 containing or lacking GTP (2 mM) and/or GdnHCl at the indicated concentrations. GdnHCl was also included in the running buffer at the same concentrations. (D) Hydrogen-deuterium exchange ratios after 7200 s incubation of 6xHis-Cdc3 in deuterated buffer were mapped onto the predicted structure of Cdc3. Color indicates exchange ratio; regions in gray were not detected by MS. Locations of the CTE, NTE, α0 helix, and G and NC interfaces are for illustration purposes only. (E) As in B, but with purified Cdc12.

region exhibited the lowest exchange ratios of any part of Cdc3, suggesting stable, efficient burial of these backbone hydrogens. Taken together, these results are most consistent with a model in which, when purified following heterologous expression in the absence of its native interaction partners, the yeast septin Cdc3 forms an unstable nonnative homodimer involving the NC interface and a CTE-mediated coiled-coil. These findings agree well with previous data in which interaction of purified 6xHis-Cdc3 with purified GST-Cdc3 required the CTE (Versele *et al.*, 2004). Notably, the only other full-length yeast septin to be previously analyzed at this level of detail, Cdc11, behaved in a similar way, forming a CTE-dependent homodimer (Brausemann *et al.*, 2016). The inability of guanidine or GTP to drive 6xHis-Cdc3 homodimerization across the G interface points to a key role for the presence of native interaction partners (chaperones or other septins) to prevent the acquisition by Cdc3 of nonnative conformations prone to nonnative interactions.

We examined Cdc12 purified in a similar way, although we had to try a number of approaches before we found one that gave sufficient yield and purity: fusion to an N-terminal maltose-binding protein-7xHis tag that was cleaved off via a TEV protease site. SEC analysis of Cdc12 at ~2 μM indicated that the majority of Cdc12 eluted as a stable homodimer of ~92 kDa, independent of added GTP (Figure 2E). A small peak corresponding to an apparent molecular weight of ~35 kDa likely represents a minor fraction of monomeric Cdc12 that, like Cdc3 monomer, eluted "smaller" than its actual size. Thus, Cdc12 is prone to nonnative homodimerization to an even greater extent than is Cdc3. Given previous results that interaction between Cdc12-6xHis and GST-Cdc12 involves the Cdc12 CTE, and that the Cdc12 CTE alone is able to weakly homo-oligomerize (Versele *et al.*, 2004), we suspect that nonnative homodimerization by purified Cdc12 is also mediated by the NC interface and coiled-coil–forming sequences in the CTE. These data provide direct evidence that, when chaperones and native interaction partners are unavailable, wild-type yeast septins adopt nonnative conformations and engage in nonnative interactions.

Chaperone requirements for posttranslational septin incorporation into native hetero-oligomers

Our finding that the absence of native interaction partners predisposes septins to nonnative conformations and interactions led us to ask whether such septins are able to make native interactions when they encounter native partners in vivo long after they are synthesized. If cytosolic chaperones cotranslationally promote native septin conformations, then individual septins synthesized in the cytosol at great excess compared with the levels of other septins may also adopt nonnative conformations and have difficulty interacting properly with other septins once those native partners become available. In other words, the excess septin may become "distracted" while it waits. Chaperones could also act posttranslationally to protect an excess septin from nonnative conformations and maintain the ability to subsequently interact with native partners long after synthesis. We used the *GAL1/10* promoter to individually overexpress single fluorescently tagged septins and monitored their ability to incorporate into septin filaments after blocking new expression by the addition of glucose (Figure 3A). Excess GFP- or mCherry-tagged molecules

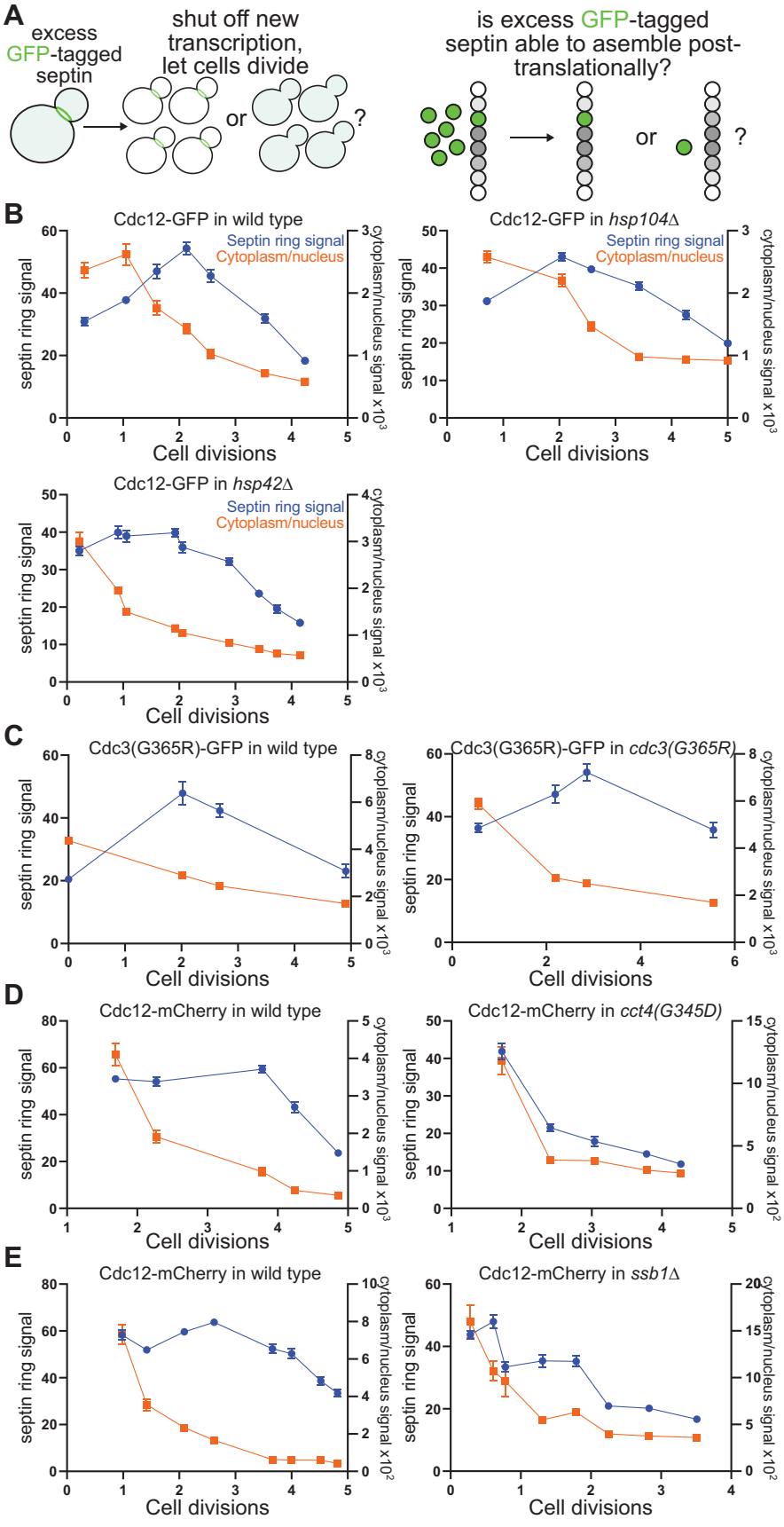

FIGURE 3: Chaperone requirements for posttranslational septin assembly. (A) Schematic illustration of experimental approach. An excess of a single, fluorescently tagged septin is generated by transient overexpression from the galactose-inducible, glucose-repressible *GAL1/10* promoter, and the fluorescent signal in septin filaments at the bud neck or in the cytoplasm/nucleus is quantified via microscopy at various time points after cessation of new expression (addition of glucose). If the excess septin is capable of assembling with newly made partner septins long after it was synthesized, then the bud neck signal should increase initially and decrease slowly thereafter via a mix of incorporation into septin filaments and dilution through cell divisions. If, on the other hand, the excess septin is unable to assemble with other septins, bud neck signal should decrease exclusively via dilution, similar to the more rapid and approximately exponential kinetics expected for the cytoplasmic/nuclear signal. (B) Wild-type diploid cells (BY4743), *hsp104Δ/hsp104Δ* mutant cells (strain 31514), or *hsp42Δhsp42Δ* mutant cells (diploid made by mating strains H00481 and H00419) carrying plasmid pMVB2 were grown in synthetic medium with 0.1% galactose and 1.9% raffinose. Following the addition of glucose to final 2%, aliquots were taken at time points and imaged (50 cells per genotype per time point). Cell concentration in the culture was also monitored at each time point to calculate the number of cell divisions following glucose addition. Points show means, error bars are SEM. (C) As in B but with haploid strain BY4741 ("wild type") or CBY07236 ("*cdc3(G365R)*") carrying plasmid pPgal-Cdc3(G365R)-GFP, and with 40 cells per genotype per time point. (D) As in C but with plasmid pGF-IVL-470 and *cct4* strain CBY11211. At least 33 cells were imaged per genotype per time point. (E) As in B but with plasmid pGF-IVL-470 and *ssb1Δ* mutant haploid cells (strain H00421). Forty cells per genotype per time point.

of Cdc3, Cdc12, or the slow-folding mutant Cdc3(G365R) accumulated in the cytoplasm/nucleus and, as cells divided without new expression of the tagged septin, cytoplasmic/nuclear signal decreased approximately exponentially with each cell division (Figure 3, B–E), consistent with dilution and negligible degradation (McMurray and Thorner, 2008). By contrast, septin ring fluorescence decreased more slowly than the cytoplasmic/nuclear signal (Figure 3, B–E), indicating that, many hours after they were translated, the excess tagged septin proteins were able to assemble into complexes capable of polymerizing into septin filaments.

We noticed fluorescent foci in a subset of cells overexpressing Cdc12-GFP (Supplemental Figure 3, A and B) and suspected that they could be aggregates of misfolded septin. However, further experiments suggested that these foci reflect properly folded Cdc12 artificially oligomerized by the GFP tag. First, the foci frequently recruited other septins, but rarely recruited the disaggregase Hsp104 (Supplemental Figure 3A). By contrast, Hsp104 colocalized

with most foci formed by overexpressing Cdc10(Asp182Asn) (Supplemental Figure 3A), a misfolding-prone mutant septin that we have previously shown to interact strongly with Hsp104 (Johnson *et al.*, 2015; Denney *et al.*, 2021). Deleting *HSP104* slightly increased Cdc12-GFP focus formation, but foci disappeared just as quickly in the absence of Hsp104 as in its presence (Supplemental Figure 3B), arguing against the idea that the foci are substrates of Hsp104 disaggregase activity. Second, while N-terminally GST-5xHis–tagged Cdc12 was also able to induce the formation of foci and long "rods" by endogenous Cdc10-mCherry, overexpressed Cdc12-mCherry did not form foci or rods (Supplemental Figure 3C).

To ask whether chaperones are required for efficient septin posttranslational hetero-oligomerization, we transiently overexpressed tagged Cdc12 in chaperone-mutant cells and monitored the kinetics of signal decay. Deleting *HSP104* did not affect the ability of excess Cdc12-GFP to incorporate into septin filaments (Figure 3B). In *cct4* cells, on the other hand, we found a clear defect in posttranslational Cdc12 incorporation, with both septin ring and cytoplasmic/nuclear signals decreasing approximately exponentially with each cell division, consistent with dilution (Figure 3D). Together with the apparent delay in de novo folding we observed in *cct4* mutants (Figure 1), we interpret these results to mean that when CCT is even slightly dysfunctional, newly made septins are 1) slower to achieve the conformation(s) required for efficient septin–septin interactions, and 2) less able to achieve and/or maintain quasinative conformations when septin–septin interactions are further delayed by a scarcity of available septin partners, as in the case of individual septin overexpression.

The enrichment of subunits of oligomeric complexes among nascent Ssb-interacting polypeptides was suggested to reflect "a potential role […] in stabilizing free subunits of oligomeric complexes, which may display a higher number of exposed contact interfaces" (Willmund *et al.*, 2013). We tested *ssb1*Δ mutants and found that, as in *cct4* cells, excess Cdc12-mCherry molecules were unable to efficiently incorporate into septin filaments long after their synthesis (Figure 3E). We noticed "leaky" expression of Cdc12-mCherry in glucose cultures of *ssb1*Δ cells (Supplemental Figure 3D), which is consistent with known glucose repression defects in *ssb* cells (Dombek *et al.*, 2004; von Plehwe *et al.*, 2009; Hübscher *et al.*, 2016) and likely explains why after glucose addition Cdc12-mCherry signal in septin rings did not decrease as rapidly as it did in *cct* cells. Thus our data likely underestimate the *ssb1*Δ septin defect. We suspect that we were able to see a defect here because in this assay the tagged septin is highly overexpressed, demanding a far greater proportion of the total cytosolic Ssb "capacity" than the low levels of tagged septin in our kinetics-of-folding assay. Consequently, an ~50% reduction in Ssb capacity due to deletion of *SSB1* alone is sufficient to generate a detectable phenotype.

We had noticed that loss of Hsp42, the general small heat shock protein of the yeast cytosol (Haslbeck *et al.*, 2004), eliminated foci of overexpressed Cdc10(Asp182Asn)-GFP (Supplemental Figure 1A), so we also tested deletion of *HSP42*. The absence of Hsp42 had no effect on posttranslational Cdc12 assembly (Figure 3B). Taken together, these results point to CCT and Ssb as chaperones that engage recently translated septins and promote conformations capable of interacting properly with partner septins long after synthesis.

In vivo site-specific cross-linking of Cdc10 to CCT

If chaperones bind with low affinity to exposed oligomerization interfaces in nascent septin proteins, preventing nonnative interactions, and are eventually "competed out" by other septins during native septin complex assembly, then we should be able to detect direct chaperones binding to those interfaces. Our genetic approach using temperature-sensitive mutants pinpointed individual residues in the G interface that, when mutated, prolong chaperone interactions (Johnson *et al.*, 2015; Denney *et al.*, 2021). However, these residues are not necessarily the sites of chaperone binding. Our previous biochemical pull down (Johnson *et al.*, 2015) and split-YFP (Denney *et al.*, 2021) studies of chaperone–septin interactions also did not directly address where exactly chaperones bind. Here, we used a site-specific cross-linking approach in living cells to address this question directly.

The genetically encoded photoactivatable amino acid *p*-benzoyl--phenylalanine (Bpa) can replace specific natural amino acids in a protein sequence in vivo (Krishnamurthy *et al.*, 2011). We introduced a UAG codon at specific locations in Cdc3 or Cdc10 and induced overexpression of either septin N-terminally tagged with GST and hexahistidine (6xHis) in yeast cells also carrying a plasmid encoding both a modified tRNA that recognizes the UAG codon and an aminoacyl-tRNA synthetase that charges the modified tRNA with Bpa (Krishnamurthy *et al.*, 2011). Sites of Bpa incorporation were chosen based on sequence-based algorithms that predict propensity for aggregation and chaperone binding sites (Figure 4A). Additionally, a nonseptin Bpa cross-linking study demonstrated that a β-hairpin is sufficient to recruit the cytosolic Hsp40 chaperone Ydj1 (Jores *et al.*, 2018). The highly conserved septin β7-β8 hairpin, which harbors the "Sep4" motif (Pan *et al.*, 2007), not only overlaps with predicted Hsp70 and Ydj1 binding sites in multiple septins, it is also buried in the septin G interface and should be exposed until a newly made septin incorporates into septin hetero-oligomers (Figure 4A).

We chose two aromatic residues for replacement with Bpa: the conserved Trp of the Sep4 "WG" sequence and a conserved Tyr in β4 between the core of the GTPase domain and the *trans* loop 1, which also makes contacts across the G interface (Weirich *et al.*, 2008). If Bpa incorporation fails, translation terminates at the UAG codon. Such premature termination can also destabilize the mRNA, so we used a yeast strain lacking Nam1/Upf1, an RNA helicase required for nonsense-mediated mRNA decay (Wang and Wang, 2008). We monitored by immunoblotting the production of full-length septins as a readout of Bpa incorporation efficiency. Bpa incorporation into Cdc10 was more efficient than for Cdc3 (Figure 4B). For both sites of Bpa incorporation into Cdc10, truncated forms were slightly more abundant than the full-length proteins (Figure 4B).

We UV-treated yeast cells expressing GST-6xHis-Cdc10 with no UAG codon or with a UAG at codon 255. Because Bpa255 should eventually become buried in the G interface with Cdc3, to avoid cross-linking only to Cdc3 and promote cross-linking to chaperones engaging nascent Cdc10, we cross-linked after 1 or 3 h of induction of expression of the tagged Cdc10. Immobilized metal affinity purification using the 6xHis tag under denaturing conditions followed by SDS–PAGE and immunoblotting with an antibody recognizing the GST tag did not reveal any obvious slower-migrating bands that would have indicated covalently cross-linked species (Figure 4C). In this experiment Bpa incorporation was much less efficient, and very little full-length protein was made. Additionally, the appearance of an ~30-kDa GST-tagged protein suggested that during the purification steps cellular proteases cleaved in the linker between the GST-6xHis portion (predicted molecular weight 31 kDa) and Cdc10 (Figure 4C).

We therefore turned to mass spectrometry to sensitively detect proteins copurifying with GST-6xHis-Cdc10(Trp255Bpa). Of a total of 856 proteins identified, 295 (34%) were found in all samples,

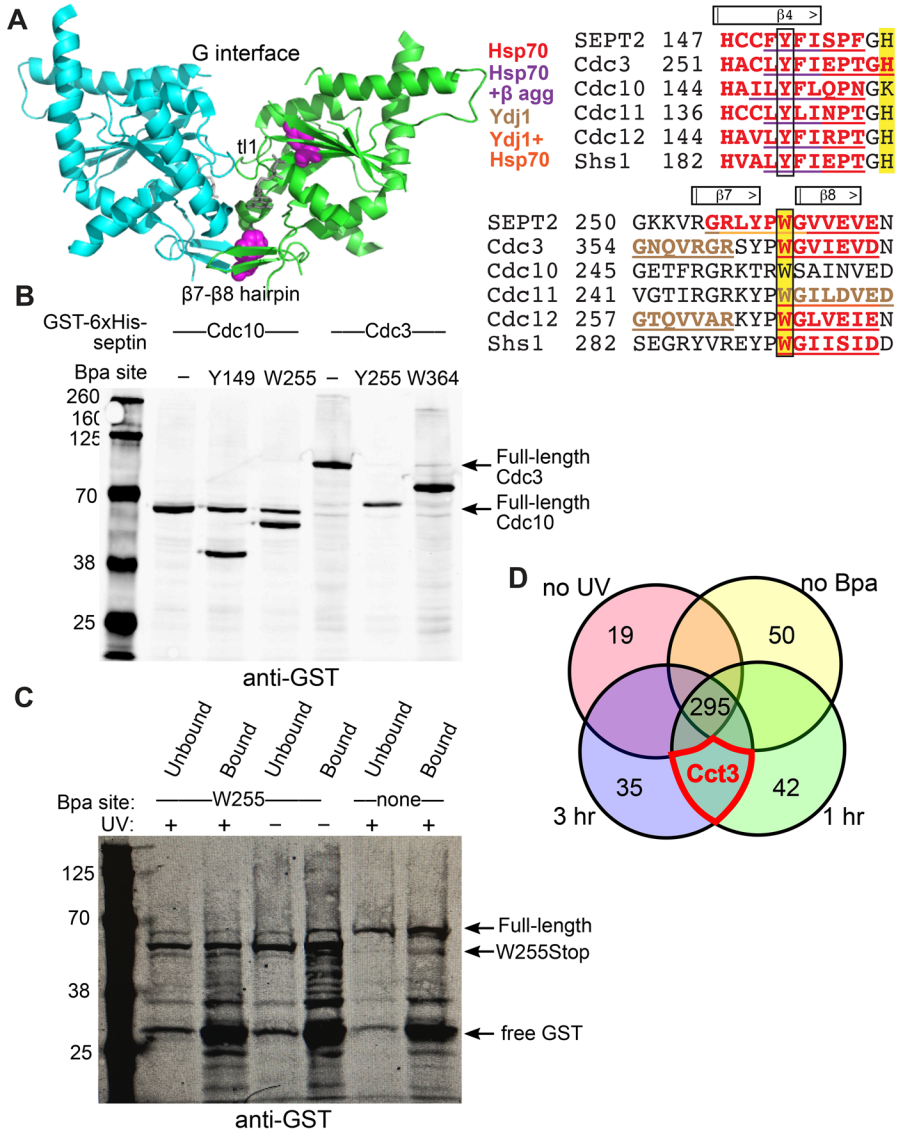

FIGURE 4: In vivo cross-linking between the chaperonin CCT and the yeast septin Cdc10. (A) Predicted chaperone binding sites. At left, ribbon structure of human septin-2 G homodimer (PDB 2QNR). Residues shown as spheres were chosen for replacement by the photocrosslinker Bpa and are boxed in the sequence alignment at right. The β7-β8 hairpin and *trans* loop 1 ("tl1") make contacts across the G interface. Predicted sites are underlined and in bold and color-coded for β-aggregation, Hsp70 and/or Ydj1. Hsp70 binding sites have LIMBO score >11.08 (Van Durme *et al.*, 2009). Ydj1-binding sites match the consensus GX[LMQ]{P}X{P}{CIMPVW} (Kota *et al.*, 2009). β-Aggregation–prone sequences are according to TANGO (Fernandez-Escamilla *et al.*, 2004). (B) Yeast cells (strain YRP2838) carrying plasmid pSNRtRNA-pBPA-RS and a plasmid encoding a GST-6xHis–tagged septin (Cdc3 or Cdc10) with or without sites of incorporation of the photocrosslinker amino acid Bpa were grown in the presence of Bpa and, to induce tagged septin expression, 2% galactose. Total protein was extracted via alkaline lysis and TCA precipitation and separated by SDS–PAGE before immunoblotting with anti-GST antibodies. (C) As in B but just for Cdc10 and cells were exposed to UV to induce cross-linking (or not, as indicated). Following protein extraction in denaturing conditions 6xHis-tagged proteins were purified by Ni-NTA affinity. (D) Venn diagram of proteins identified by mass spectrometry in samples prepared as in C. Circles are not drawn to scale. Numbers indicate numbers of unique proteins identified; there were two independent biological replicates of all samples except the no-UV sample. For this diagram, the replicates were pooled together. Cct3 was the only protein identified in all experimental samples and none of the controls. "No Bpa" means wild-type Cdc10, with no UAG codon for Bpa incorporation.

including the negative controls (two replicates of wild-type GST-6xHis-Cdc10 and one sample with GST-6xHis-Cdc10(Trp255Bpa) but no exposure to UV; Figure 4D and Supplemental Table 1). These proteins included Cdc10, as expected; most others are expected to be highly abundant in galactose-grown yeast cells (Pgk1, Gal10, Gal7, ribosomal proteins, etc.). A single protein was absent from all negative controls and present in both time points of both independent biological replicates of samples containing GST-6xHis-Cdc10(Trp255Bpa). That protein was the CCT subunit Cct3 (Figure 4D and Supplemental Table 1).

Other chaperones may have cross-linked to Cdc10, but were also found in negative controls. For example, Hsp104, Ssa1, Ssb1, Sis1, and Ydj1 were all found in multiple experimental samples but also in multiple negative controls (Supplemental Table 1). These chaperones are very abundant in the cytoplasm (Brownridge *et al.*, 2013) and are commonly found bound nonspecifically to affinity purification media (Mellacheruvu *et al.*, 2013). Thus one caveat of our approach is that some Cdc10-binding chaperones were likely missed as "false negatives." Nonetheless, these data support our model that CCT binds directly in a nascent septin to a future septin–septin interaction interface, consistent with a chaperonin role in cotranslational septin folding.

In vivo site-specific cross-linking of Cdc10 to GroEL

Our findings described above support a model in which chaperonin function is important for de novo septin folding and that this function involves direct chaperonin binding to nascent septins. A previous study dismissed a role for CCT in de novo septin folding because septins fold properly in *E. coli* (Dekker *et al.*, 2008), which lacks CCT and instead has a distantly related chaperonin, GroEL. CCT and GroEL differ in many ways, and GroEL cannot substitute for CCT for the folding of other cytosolic nucleotide-binding cytoskeletal proteins (actin and tubulins [Tian *et al.*, 1995a; Balchin *et al.*, 2018]). Nonetheless, GroEL binds Cdc10 in an *E. coli* lysate-based in vitro translation reaction; adding purified CCT displaces Cdc10 from GroEL and creates a CCT–Cdc10 complex (Dekker *et al.*, 2008). Thus an alternative explanation for the lack in those experiments of any CCT effect on Cdc10 conformation in those experiments (as assessed by native PAGE) is that either chaperonin was sufficient to direct

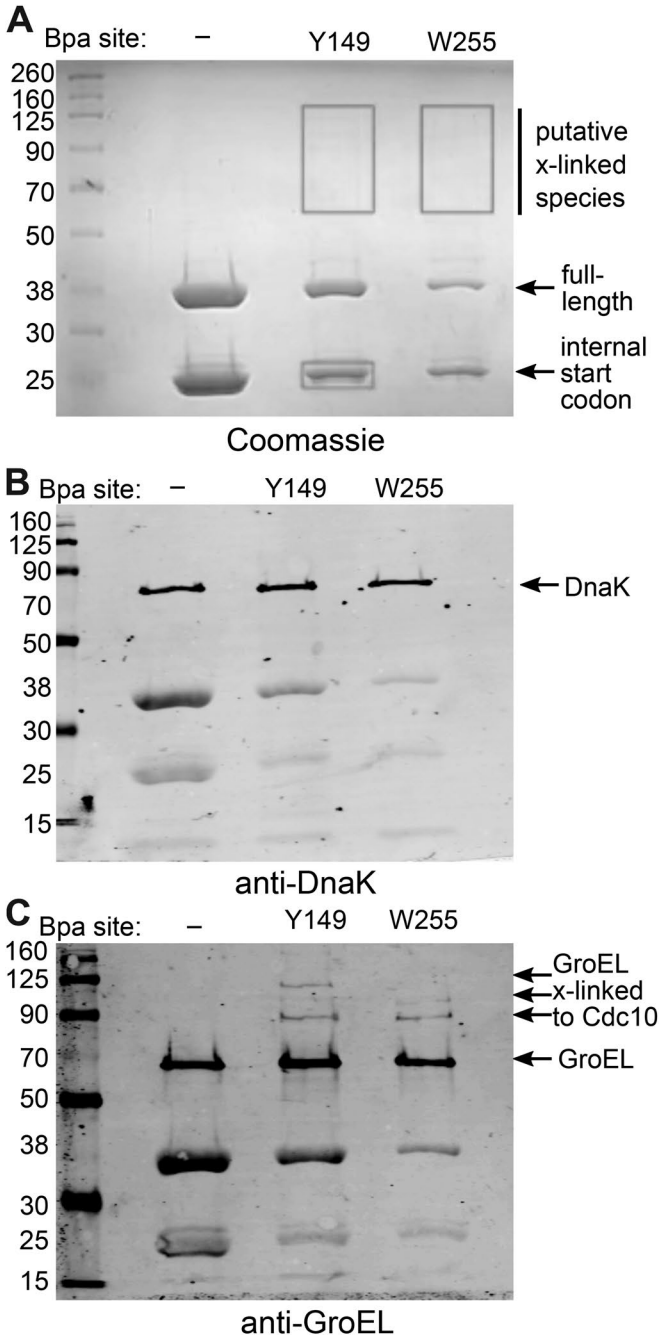

FIGURE 5: In vivo cross-linking between the *E. coli* chaperonin GroEL and the yeast septin Cdc10. (A) *E. coli* cells (strain BL21(DE3)) carrying plasmid pEVOL-pBpF and a Cdc10-6xHis plasmid with the indicated site of Bpa incorporation were grown in the presence of Bpa. IPTG was added to induce tagged Cdc10 expression and cells were exposed to UV and then lysed in denaturing conditions. Proteins bound to Ni-NTA were separated by SDS–PAGE and stained with Coomassie. Boxes indicate regions of the gel that were excised for mass spectrometry. (B, C) Samples as in A were separated by SDS–PAGE and then immunoblotted for DnaK (B) or GroEL (C). The leftmost lanes in all gels contained molecular weight ladder (Li-Cor Biosciences # 928-60000).

Cdc10-folding. To look for evidence that GroEL directly interacts with Cdc10 in vivo at the same sites as does CCT, we adapted our Bpa cross-linking approach for *E. coli*.

We introduced into BL21(DE3) cells a plasmid encoding Cdc10 with a C-terminal 6xHis tag and a UAG codon at position 149 or 255 and a plasmid encoding the appropriate modified tRNA and aminoacyl-tRNA synthetase. Cross-linking was performed following induction of Cdc10-6xHis expression with isopropyl β-D-1-thiogalactopyranoside (IPTG) in the presence of Bpa, followed by affinity purification under denaturing conditions and visualization by SDS–PAGE and Coomassie staining (Figure 5A). We expected that the use of a C-terminal affinity tag would guarantee purification of only full-length Cdc10 (37 kDa), but a band of ~29 kDa was nearly as abundant and was also present in a control sample with no UAG codon (Figure 5A). This band was excised from the gel and subjected to mass spectrometry, the results of which suggested that this product arose from translation initiation at an internal AUG codon corresponding to Met77 in full-length Cdc10 (Supplemental Figure 4). Bands migrating slower than full-length Cdc10-6xHis were faintly visible only in the samples in which Bpa was incorporated into Cdc10 (Figure 5A). Mass spectrometry identified multiple *E. coli* chaperones in the part of the gel that included these bands, including GroEL and the Hsp70 DnaK (Supplemental Table 2). Both chaperones are highly abundant and are common nonspecific contaminants of affinity purifications (Bolanos-Garcia and Davies, 2006; Robichon *et al.*, 2011). We analyzed the same samples by immunoblot using anti-GroEL or anti-DnaK antibodies. Only GroEL was present in slowly migrating, Bpa-dependent bands (Figure 5, B and C). Thus both CCT and GroEL directly interact at the same site in the septin Cdc10.

GroEL dysfunction inhibits heterologous production of the yeast septin Cdc12

Our findings that GroEL and CCT bind a septin at the same site are consistent with a model in which septin folding in *E. coli* involves GroEL. To ask directly about *E. coli* chaperone requirements for yeast septin folding, we mutated cytosolic chaperones in *E. coli* and looked for defects in hetero-oligomerization by heterologously expressed yeast septins. On the basis of our previous yeast septin-chaperone interaction results (Johnson *et al.*, 2015; Denney *et al.*, 2021), we focused on ClpB (homologue of the disaggregase Hsp104), DnaJ (major cytosolic Hsp40), DnaK (sole cytosolic Hsp70), GroEL, and HtpG (sole cytosolic Hsp90).

For Δ*clpB* and Δ*htpG* we obtained *E. coli* deletion strains (Baba *et al.*, 2006) representing these nonessential chaperones and lysogenized them with the DE3 prophage to allow T7 RNA polymerase expression upon addition of IPTG. Because DnaJ and DnaK are required for efficient phage replication (Yochem *et al.*, 1978), we first lysogenized the wild-type parent strain of the *E. coli* deletion collection and then introduced Δ*dnaJ* or Δ*dnaK* alleles by recombination. In all four deletion strains we took extra steps to rule out the acquisition of extragenic suppressors or the persistence of wild-type alleles (see *Materials and Methods*). We then introduced two plasmids, each encoding two yeast septins (Cdc10 and 6xHis-tagged Cdc12 or Cdc3 and Cdc11) under control of the T7 promoter. For GroEL, we used a Δ*groEL* strain carrying three plasmids: one encoding the temperature-sensitive *groEL(Glu461Lys)* mutant allele (Chapman *et al.*, 2006), one encoding T7 RNA polymerase under control of the IPTG-inducible *lac* promoter, and one encoding untagged Cdc3 and 6xHis-tagged Cdc12 under T7 promoter control. Cells were grown at 24°C to mid–log phase and subsequently induced with IPTG at 24°C or 37°C. Following cell lysis, 6xHis-Cdc12 was purified from the soluble fraction and stoichiometric copurification of the other, untagged septins was taken as evidence of proper septin folding and complex assembly. Stoichiometric septin

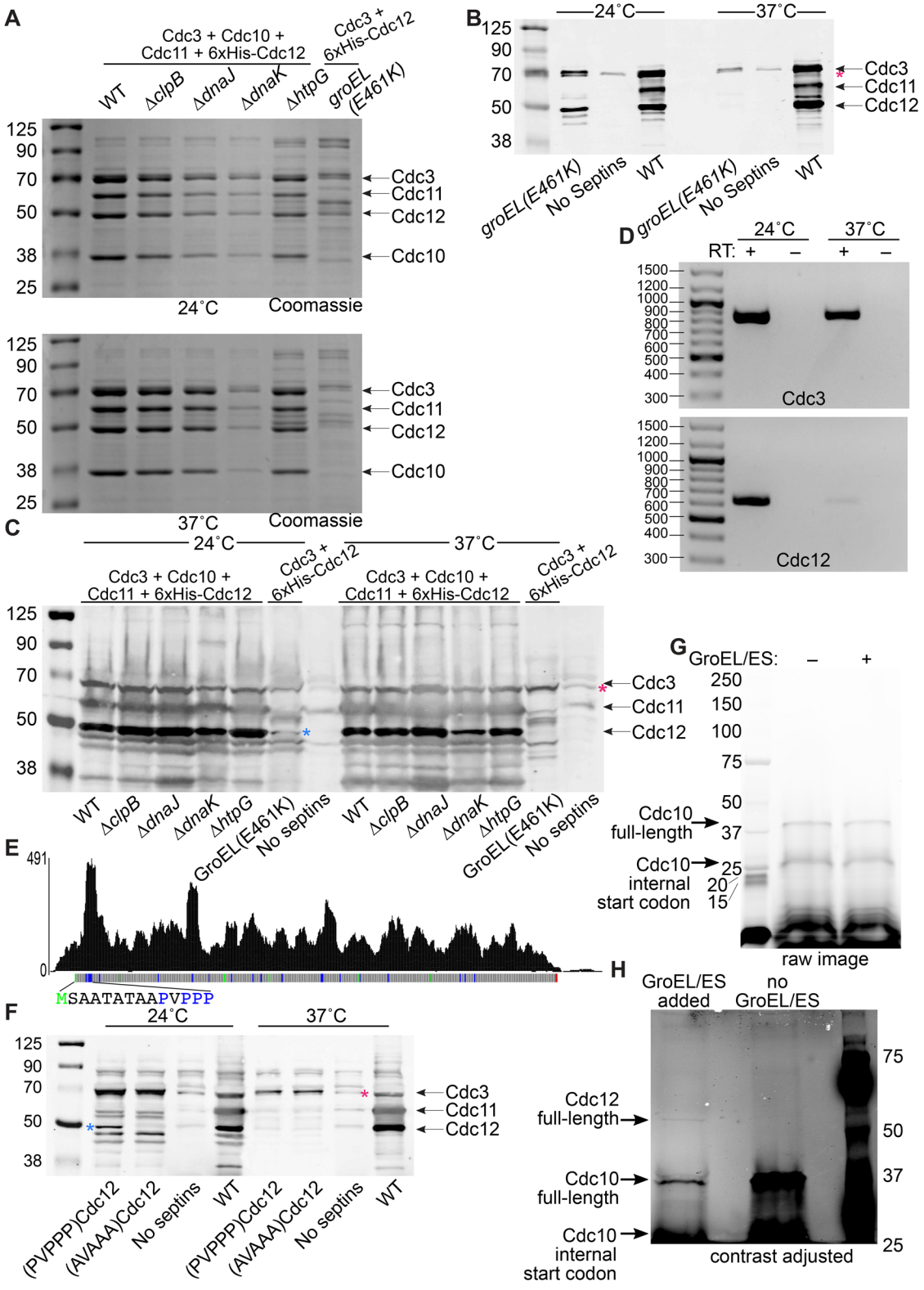

FIGURE 6: Chaperonin requirement for translation of the septin Cdc12 by prokaryotic ribosomes. (A) Coomassie-stained SDS–PAGE of proteins purified via Ni-NTA from wild-type or *groEL*-mutant *E. coli* cells carrying plasmids encoding the indicated septins, plus other plasmids as necessary for induction or viability. Strains were B002 ("WT"), B003 ("Δ*clpB*"), B004 ("Δ*dnaJ*"), B005 ("Δ*dnaK*"), B006 ("Δ*htpG*"), and 461 ("*groEL(E461K)*"). Septin-encoding plasmids were pMVB128, pMVB133, and pMAM54. Leftmost lane contains a molecular weight ladder (Li-Cor Biosciences #928-60000). (B) Immunoblot of bound proteins prepared as in A, plus a sample from wild-type cells (B002) carrying no septin-encoding plasmid ("No Septins"), using a cocktail of antibodies recognizing Cdc3, Cdc11, and the 6xHis tag. Magenta asterisk indicates an ~70 kDa protein weakly reactive with the Cdc3 and/or Cdc11 antibody. (C) As in B but for urea-solubilized pellets (cell debris and insoluble material) obtained following cell lysis. The blue asterisk indicates the

complexes were obtained from Δ*clpB*, Δ*dnaJ*, Δ*dnaK*, and Δ*htpG* cells (Figure 6A), indicating that these chaperones are not strictly required for de novo septin folding, at least in this context. Reductions in the total yield of septin complexes in several mutants (Figure 6A) likely reflect defects in transcriptional induction, rather than in septin translation or folding, because similar reductions were seen for expression of a control protein (see *Materials and Methods*).

By contrast, in the *groEL*-mutant cells, bands at the positions expected for Cdc3 and 6xHis-Cdc12 were visible in Coomassie-stained samples from cells induced at 24°C but not at 37°C (Figure 6A). Because we saw multiple other proteins of unexpected sizes in the bead-bound samples, to improve our detection of septin expression we used immunoblotting and antibodies recognizing Cdc3 or the 6xHis tag. These experiments confirmed that, while Cdc3 was present in cells induced at either temperature, 6xHis-Cdc12 was found only in cells induced at 24°C (Figure 6B). Because Cdc12 was also missing from urea-solubilized pellets (Figure 6C), its absence from bead-bound samples was not the result of Cdc12 aggregation/insolubility. These findings suggested that severe GroEL dysfunction perturbs Cdc12 translation. Poor translation of non–*E. coli* proteins heterologously expressed in *E. coli* is frequently accompanied by loss of the mRNA (Boël *et al.*, 2016). Indeed, we found that whereas Cdc3 mRNA was present at similar levels in *groEL*-mutant cells induced at either temperature, 6xHis-Cdc12 mRNA was barely detectable at 37°C (Figure 6D). These results point to a specific defect in Cdc12 translation upon GroEL dysfunction, leading to turnover of the Cdc12 mRNA, consistent with a cotranslational requirement for GroEL in Cdc12 folding.

A cluster of prolines near the N-terminus promote Cdc12 translation in *groEL*-mutant *E. coli*

Our findings indicated that Cdc12 is more sensitive than Cdc3 to GroEL dysfunction. We considered several possible explanations. Defects in cotranslational folding in *E. coli* due to chaperone mutations are known to cause premature termination of translation of some endogenous proteins via recruitment of the ribosome release factor RF3 (Zhao *et al.*, 2021), but it was not obvious why Cdc12 would be affected more than Cdc3. mRNA degradation is also not known to follow RF3 recruitment. mRNA degradation does accompany translation defects when proteins enriched in "suboptimal" codons are heterologously expressed in *E. coli* (Boël *et al.*, 2016). Moreover, obligate GroEL clients appear to accumulate suboptimal codons over evolutionary time, suggesting that assistance from GroEL is able to overcome otherwise deleterious effects of codon content on translation and folding (Warnecke and Hurst, 2010). If Cdc12 is enriched for suboptimal codons compared with Cdc3, this might explain the more severe effect of GroEL dysfunction on Cdc12. However, we found no obvious differences in the predicted "codon adaptation index" of Cdc3 versus Cdc12 (Supplemental Figure 5A). Cdc12 also has none of the 17 pairs of adjacent codons that reduce translation (Gamble *et al.*, 2016). mRNA secondary structure within the open reading frame (ORF) correlates with slower translation elongation (Burkhardt *et al.*, 2017), but predictions of ORF mRNA secondary structures for Cdc12 and Cdc3 did not reveal any clear differences (Supplemental Figure 5B). We looked for specific pairs of amino acids (Ahmed *et al.*, 2020) known to induce translational pausing in yeast, but again found no clear difference between the two septins (Supplemental Figure 5C). Thus most established causes of defects in translation could not explain the heightened sensitivity of Cdc12 to GroEL dysfunction.

Finally, we considered charge. Positively charged residues, especially Arg, and overall charge, as indicated by isoelectric point, correlate with slow translation of yeast proteins (Riba *et al.*, 2019), presumably due to electrostatic interactions with the negatively charged ribosome exit tunnel (Lu and Deutsch, 2008; Charneski and Hurst, 2013). Cdc12 has nearly twice the number of Arg residues (29) than does Cdc3 (17), despite being ~30% shorter (Supplemental Figure 5C), and has a much higher isoelectric point (pI; 8.23 vs. 5.14). An enrichment of positively charged amino acids in Cdc12 could result in slowly moving, closely spaced ribosomes on the body of the Cdc12 mRNA. Indeed, published yeast polysome profiling experiments found that the density of ribosomes per 100 nucleotides on Cdc12 mRNA (0.87) is nearly twice that of Cdc3 (0.45) (Arava *et al.*, 2003). Closely spaced ribosomes would put Cdc12 at high risk for stall-induced ribosome collision and consequent degradation of the mRNA and nascent protein. Single-molecule experiments show that the free energy drop accompanying cotranslational folding can overcome ribosome stalling (Goldman *et al.*, 2015). Thus Cdc12 would be more sensitive than Cdc3 to the loss of pulling force from GroEL-assisted cotranslational folding in *groEL*-mutant cells.

Searching for support for this model, we noticed in published yeast ribosome profiling data (Sen *et al.*, 2015) that the major peak of ribosome accumulation on Cdc12 mRNA is at a Pro-rich cluster (ProValProProPro) located near the N-terminus (Figure 6E). Pro residues are intrinsically difficult to translate (Pavlov *et al.*, 2009). We reasoned that, like the "translational ramp" observed for many proteins in diverse species (Fredrick and Ibba, 2010), ribosome accumulation on the Pro-rich cluster at the Cdc12 N-terminus may act to promote regular spacing of ribosomes downstream, preventing collisions. Indeed, a very recent study showed that a cluster of slowly translated codons near the start codon stabilizes mRNAs with

band corresponding to Cdc12. (D) DNA agarose gel electrophoresis and ethidium bromide staining of products of RT-PCR for Cdc3 or Cdc12 mRNA from total RNA extracted from *groEL*-mutant strain 461 carrying plasmid pMAM54 and induced with IPTG at the indicated temperatures. The presence or absence of reverse transcriptase ("RT") in the reactions is indicated. Leftmost lane contains molecular weight ladder (Thermo Fisher Scientific #SM0331). (E) Published Ribo-seq/ribosome profiling data (Sen *et al.*, 2015) showing the positions of ribosomes along the Cdc12 mRNA as numbers of reads of ribosome-protected mRNA fragments. Below, the Cdc12 ORF is illustrated with Met codons in green, Pro codons in blue, and the stop codon in red. The first 14 amino acids of Cdc12 are indicated with the same color scheme. (F) As in B but including samples from *groEL*-mutant cells carrying the plasmid pMAM88, which encodes Cdc3 and 6xHis-tagged Cdc12 with the four Pro residues highlighted in E mutated to Ala ("(AVAAA)Cdc12"). Samples from cells with pMAM54, encoding wild-type Cdc12, are indicated by "(PVPPP)Cdc12." The blue asterisk indicates the band corresponding to Cdc12. (G) Chaperone-free in vitro transcription/translation reactions lacking release factors (PURExpress ΔRF123) and containing fluorescent puromycin to label translation products were resolved by SDS–PAGE. The template plasmid pMVB128 encodes Cdc10 and 6xHis-Cdc12. Purified GroEL/ES chaperonin was added to one reaction, as indicated. Leftmost lane contains a molecular weight ladder (Bio-Rad #1610395). (H) As in G but gel was run longer, the order of lanes is reversed, and brightness and contrast were adjusted in FIJI.

downstream slowdowns, presumably by preventing ribosome "traffic jams" (Sharma *et al.*, 2021). To test this model, we mutated all of the Pro residues in the cluster to Ala, which should tighten ribosome spacing on the main body of Cdc12 mRNA, favoring ribosome collisions when GroEL is even slightly dysfunctional.

As predicted by our model, eliminating the Pro-rich cluster exacerbated the Cdc12 synthesis defect: no mutant Cdc12 was detectable at 24°C, a temperature permissive for culture growth and for synthesis of Cdc3 and wild-type Cdc12 (Figure 6F). The Pro-mutant Cdc12 was translated efficiently and folded normally in wild-type *E. coli*, as evidenced by copurification with coexpressed Cdc3 (Supplemental Figure 6). Note that the Glu461Lys mutation perturbs GroEL function to some extent at all temperatures, because mutant cells are unable to proliferate in minimal medium at any temperature (Horwich *et al.*, 1993). We interpret these results as indicating that whereas translation of wild-type Cdc12 fails only when GroEL is completely nonfunctional (in *groEL(E461K)* cells at 37°C), translation of the mutant Cdc12 lacking the Pro-rich cluster fails when GroEL is only slightly dysfunctional (in *groEL(E461K)* cells at 24°C). Thus the Pro-rich cluster in Cdc12 confers protection from translation failure associated with GroEL dysfunction, consistent with slow Cdc12 translational elongation driving a requirement for chaperonin assistance in translation.

GroEL/ES is sufficient to promote Cdc12 translation during cell- and chaperone-free in vitro translation

To further test our model that the lack of Cdc12 protein synthesis in *groEL*-mutant cells reflects intrinsic difficulties in translating Cdc12 protein without functional GroEL, we attempted to synthesize Cdc12 in the context of a cell- and chaperone-free in vitro translation system based on components purified from *E. coli* (Shimizu *et al.*, 2001). The PURExpress system has been used previously to demonstrate cotranslational action of GroEL on an established client protein (Ying *et al.*, 2006). To specifically detect translation products, we used a version of this system lacking ribosome release factors and added fluorescently labeled puromycin at a low concentration, which results in covalent C-terminal fluorescence labeling of translation products (Kawahashi *et al.*, 2007). Cdc12 and Cdc10 mRNAs were generated in the same reactions using T7 RNA polymerase and a plasmid encoding both Cdc12 and Cdc10, each under control of a T7 promoter. We saw fluorescent bands corresponding to the size of full-length Cdc10 (~37 kDa) and the short version of Cdc10 made from the internal start codon (~29 kDa) but nothing the size of full-length Cdc12 (~49 kDa) (Figure 6G), providing an independent demonstration that Cdc12 is more sensitive than other yeast septins to the absence of GroEL. Note that the pI of Cdc10, 5.47, is similar to that of Cdc3.

To ask whether GroEL folding activity is sufficient to restore Cdc12 translation, we obtained purified GroEL and GroES (a cochaperonin protein required for full GroEL folding activity [Goloubinoff *et al.*, 1989a,b]) from a commercial source, verified in vitro ATPase activity and folding activity of the reconstituted holoenzyme on a known client (Supplemental Figure 7), and added it to the septin synthesis reactions. Upon the addition of GroEL/ES, we saw a faint fluorescent band the size of full-length Cdc12 (Figure 6G). Using mass spectrometry, we detected peptides at or near the C-termini of Cdc10 and Cdc12 in a GroEL/ES-supplemented reaction (Supplemental Figure 8A and Supplemental Table 3), confirming the production of full-length Cdc10 and Cdc12. Notably, we also found a few peptides from DnaK, presumably a contaminant of the purified GroEL and/or GroES (Supplemental Figure 8A and Supplemental Table 3). We further note that because RF3 is among the release factors missing from these reactions, RF3 recruitment to ribosomes translating Cdc12 cannot explain the defect in Cdc12 synthesis in the absence of GroEL.

The conserved bacterial elongation factor P (EF-P) is required for efficient translation of proteins containing Pro-rich clusters in vivo and in the same kinds of cell-free in vitro reactions that we used (Ude *et al.*, 2013). To determine to what extent the absence of EF-P from the reactions contributed to defects in Cdc12 translation, we obtained EF-P from a commercial source, added it to reactions, and saw no effect (Supplemental Figure 8B). The lack of a detectable effect of EF-P on Cdc12 was not entirely unexpected, considering that for a different protein with a very similar Pro-rich cluster (ProProProllePro), an EF-P effect was apparent only at very short reaction times (Ude *et al.*, 2013). Only ~85 endogenous *E. coli* proteins strictly require GroEL for de novo folding; for most GroEL clients, other chaperones like trigger factor and/or DnaK can compensate to some extent for the loss of GroEL (Kerner *et al.*, 2005), and vice versa (Zhao *et al.*, 2021). We suspect that the lack of these other chaperones from the in vitro reactions explains why adding GroEL/ES was able to support only a low yield of Cdc12.

Taken together with other findings, these observations provide direct, independent support for a model in which all septins benefit from cotranslational folding assistance from a subset of cytosolic chaperones, including a chaperonin, with Cdc12 being especially sensitive to defects in chaperonin function.

DISCUSSION

It is easy to imagine that protein quaternary structure arises directly and spontaneously from proper tertiary structure, but reality is more complicated, especially in living cells. Because native tertiary structure is often achieved only in the context of quaternary structure, the two are not easily resolved. We focus on septin proteins, which are both more complex and less studied than other, simpler cytoskeletal proteins like the tubulin heterodimer. More subunits per complex (up to eight) and a propensity for homo-oligomerization means that there are many "wrong" ways to assemble septin subunits, such as what happened in early in vitro studies of purified budding yeast septins (Versele *et al.*, 2004). In the end, the purified complexes that revealed the true subunit organization within septin complexes were made either by coexpression of all the subunits in the same cells (Bertin *et al.*, 2008) or, tellingly, by expression of different subunits in different cells and mixing the cells together during cell lysis (Mendonça *et al.*, 2019, 2021). The failure to achieve native assembly when mixing purified septins compared with the success when coexpressing septins or mixing cells points to some cellular factor(s) important for native septin assembly. Our findings provide evidence that those factors are cytosolic chaperones.

Our observations of apparent septin folding defects in *cct* and *ssb* mutants fit well with proposed functions of CCT and Ssb in cotranslationally engaging free subunits of multiprotein assemblies. A class of nonseptin CCT clients enriched in subunits of protein complexes bind relatively slowly to the chaperonin during their translation, which was suggested to reflect "the action of cooperating upstream chaperones delaying binding to [CCT] during translation" and client "accumulation" on CCT before "release into oligomeric assemblies" (Yam *et al.*, 2008). By identifying the ribosome location on an mRNA when the nascent protein is bound by chaperones, selective ribosome profiling experiments reveal how much of the protein has emerged from the ribosome exit tunnel when a chaperone binds and can provide information about which chaperones act "upstream" of others (Stein *et al.*, 2019). In this assay, Cdc3 was the only septin that reached the most conservative

confidence threshold for CCT binding, whereas Cdc3, Cdc10, Cdc11, and Cdc12 were all confidently identified as cotranslationally bound by the more abundant Ssb (Stein *et al.*, 2019). Whereas for most nonseptin proteins Ssb bound to sites translated earlier than to the sites bound by CCT, Ssb and CCT both bound transiently to Cdc3 just as the α2 helix was emerging from the tunnel (Stein *et al.*, 2019) (Supplemental Figure 9). Ssb also bound Cdc10 at the equivalent location (Supplemental Figure 9). In natively folded Cdc3, α2 covers an otherwise exposed surface made by the previously translated β1 and β3 strands (Supplemental Figure 9). This CCT binding pattern to Cdc3 perfectly matches the pattern noted by Stein *et al.* (2019) for other proteins with α-β sandwich Rossmann folds, where once the α helix is completely translated, it buries the exposed surface and displaces CCT. Notably, in our HDX-MS studies of purified Cdc3 the β1 strand was largely exposed to solvent (Figure 2D and Supplemental Figure 2), consistent with a model in which "free" septins continuously attract the attention of CCT or Ssb, even when fully translated. The sites in Cdc10 where we introduced Bpa and observed chaperonin cross-linking would not yet be translated when this first binding event occurs (Supplemental Figure 9). We presume that either these sites are bound too transiently by CCT to be detected by selective ribosome profiling or our cross-linking reflects "incidental" chaperonin contacts, for example with the chamber walls rather than the apical domains (see below).

Together with our findings, these insights from the recent literature led us to a model in which nascent septins are engaged cotranslationally by both Ssb and CCT at the same locations (Figure 7). Ssb1 or Ssb2 are presumably in complex with their J-protein partner, Zuotin/Zuo1 (Yan *et al.*, 1998), and the "atypical" Hsp70 Ssz1 (Lee *et al.*, 2021), which does not bind septins (Denney *et al.*, 2021) (Figure 7). Early septin folding steps bury the sequences that recruited Ssb, triggering Ssb release and allowing engagement by CCT, which recognizes a septin conformation nearer to the native state. ATP hydrolysis by CCT releases a quasinative septin from the chaperonin chamber and, if a partner septin is available for interaction, the partner septin occupies the site of CCT binding and prevents further rounds of CCT engagement (Figure 7). If no partner septin is available, rounds of CCT and/or Ssb binding and release continue until one is. CCT or Ssb dysfunction inhibits posttranslational septin assembly because the "free" septin falls into kinetic traps—nonnative, low-free-energy conformations that are not competent for septin–septin interaction and are susceptible to prolonged association with other chaperones as well as nonnative intramolecular interactions. We note that whereas the failure of a "free" subunit to fold efficiently and bind stably to assembly partners targets many other kinds of proteins for proteolytic degradation (Goldberg and Dice, 1974; Goldberg, 2003), yeast septins somehow evade this fate. One possible explanation is that "free" septins are in sufficiently nearnative conformations that—like stably misfolded intermediates adopted by half of wild-type *E. coli* proteins (Nissley *et al.*, 2022)—bypass the proteolytic machinery.

Generally speaking, Ssa chaperones interact with nascent chains but to a lesser extent than do Ssb and CCT (Albanèse *et al.*, 2006), so Ssa4 may act downstream of Ssb and CCT to promote efficient septin folding (Figure 7). The folding delay in *ssa4*Δ but not *ssa1*Δ cells is consistent with our physical septin-chaperone interaction assays (Denney *et al.*, 2021) and, because under nonstress conditions Ssa4 is ~60-fold less abundant than Ssa1 (Brownridge *et al.*, 2013), points to functional specificity that is also consistent with specificity of genetic interactions, phenotypes, and transcript-level changes in different *ssa* mutants (Hasin *et al.*, 2014; Lotz *et al.*, 2019).

As a way of explaining how slow-folding mutant septins are so efficiently excluded from assembly into septin complexes in cells also expressing a wild-type version of the same septin, we previously proposed that the G1 phase of the cell cycle represents a "window of opportunity" for septin complex assembly (Schaefer *et al.*, 2016). According to our model, if a mutant septin has not already incorporated into septin hetero-octamers by the end of G1, it is unable to do so thereafter and is found primarily in the cytosol/nucleus, presumably bound by chaperones (Johnson *et al.*, 2015; Schaefer *et al.*, 2016). Because we use cell divisions to mark time passed since synthesis, this model predicts that a slow-folding mutant septin would be unable to assemble posttranslationally in our assay. Our results with Cdc3(Gly365Arg)-GFP were inconsistent with this prediction. We previously showed that the Cdc3 NTE protects another G-interface mutant, Asp289Asn, from being "outcompeted" by wild-type Cdc3 during assembly into septin complexes, likely because it shields the G interface from binding to specific chaperones that would otherwise inhibit interactions between the mutant Cdc3 and its G dimer partner, Cdc10 (Weems and McMurray, 2017). We note that while our split-YFP results pointed to a few differences in the way cytosolic chaperones interact with Cdc3 compared with the other septins, all bound to Ssb and at least one subunit of CCT (Denney *et al.*, 2021). We interpret these differences in septin behavior as evidence that while special septin features like an NTE may alter interactions with some chaperones and influence the ability of a mutant septin to compete with its wild-type counterpart—i.e., in the context of "quality control"—Ssb, CCT, and Ssa2-4 likely promote the folding of all wild-type septins.

Our in vivo cross-linking studies and the selective ribosome profiling results (Stein *et al.*, 2019) showing that chaperonins directly bind residues at or near the septin–septin G interface fit with our previous findings that mutations in or near the G interface generally prolong chaperone binding, presumably by delaying the acquisition of the native conformation capable of binding another septin and thereby rendering the sites inaccessible to chaperones. Because we did not test them, we cannot rule out other binding sites. It makes intuitive sense, however, that the septin NC interface, which at least for Cdc11 and Shs1 is exposed at both ends of a septin octamer, would not attract much cytosolic chaperone attention. A recent study that cross-linked Lys residues (Nitika *et al.*, 2021) found a direct interaction between Ssa1 and a Lys (478) in the CTE of Cdc3, far from the G and NC interfaces (Supplemental Figure 10) and within the putative coiled-coil formed in the nonnative G Cdc3 homodimer (Figure 2). These cross-links with Ssa1 probably occurred only because the other Ssa chaperones were eliminated (Nitika *et al.*, 2021); otherwise Ssa2, Ssa3, or Ssa4 would presumably have "outcompeted" Ssa1 for septin interaction. As the cross-linked lysine in Ssa1 lies on the surface of the lid of the substrate-binding domain, it is possible that, once the Cdc3 NTE is displaced by interaction with Cdc12, the Ssa1 substrate-binding pocket does engage the Cdc3 G interface, bringing the Lys-rich Cdc3 CTE near the Ssa1 lid (Supplemental Figure 10).

In terms of CCT binding, if the client peptides bind in opposite orientations, the pattern of polar and hydrophobic residues in the Cdc10 sequence surrounding Trp255 (RGRKTRWSAINVED, in single-letter code), where Bpa substitution yielded cross-links to Cct3, resembles the part of the HIV p6 protein (DKELYPLTSLRSLFGN) contacted by the apical domain of human Cct3 (Joachimiak *et al.*, 2014). Each CCT subunit has a distinct binding specificity (Joachimiak *et al.*, 2014; Balchin *et al.*, 2018) and, as indicated by our split-YFP

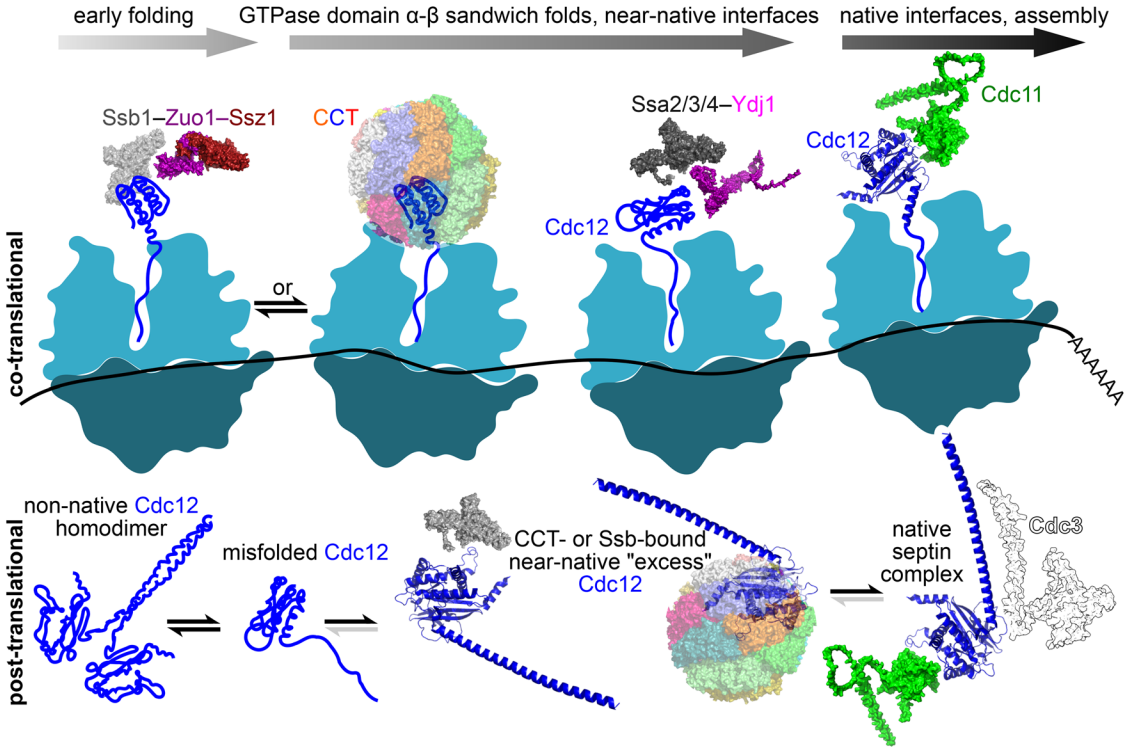

FIGURE 7: Model for cotranslational chaperone-mediated septin folding in the context of septin complex assembly. In this illustration, folding and translation proceed from left to right. CCT and Ssb (Ssb1 or Ssb2) initially interact with the same exposed surface composed of strands β1 and β3 from the α-β sandwich, until α is synthesized and buries that surface. Not shown: CCT may also bind later at the β4 and/or β7-β8 hairpin, as evidenced by our in vivo photocrosslinking. Ssa-family chaperones (but not Ssa1) interact with nascent Cdc12 to promote native folding until Cdc12 has achieved a conformation capable of stably interacting with partner septins. Ydj1 is shown as the presumptive Hsp40 for Ssa. If folded Cdc11 is available during Cdc12 translation, a Cdc12–Cdc11 heterodimer assembles cotranslationally ("co-translational"). Alternatively, if Cdc12 is in excess to other septins, it completes translation without having interacted with another septin ("post-translational"). Here, Cdc12 is susceptible to "off-pathway" nonnative conformations prone to nonnative homodimerization. CCT and Ssb continue to interact with full-length Cdc12 (as illustrated), inhibiting off-pathway conformations until stable septin complexes assemble. Not illustrated: their dysfunction during translation produces full-length Cdc12 that is irreversibly misfolded and has no path to stable septin assembly. Other septins presumably require similar chaperone assistance for de novo folding but Cdc12 is the slowest to be translated and thus a potential "platform" for cotranslational assembly. Protein structures are AlphaFold predictions (the NTE of Cdc3 is hidden, for clarity) or cryo-EM structures (human CCT; PDB 7LUM [Knowlton *et al.*, 2021]; Zuo1–Ssz1, PDB 7 × 3K [Chen *et al.*, 2022]).

studies (Denney *et al.*, 2021), despite overall structural similarity different septins are likely contacted by different combinations of CCT subunits within the folding chamber. GroEL, too, relies on a distribution of polar and nonpolar surfaces to bind its clients (Chen and Sigler, 1999). Known sites of GroEL binding in other proteins (Wang *et al.*, 1999) also match the highly hydrophobic sequence surrounding Cdc10(Tyr149Bpa) (Figure 4A), which also cross-linked to GroEL. Nonetheless, as with the Ssa1 example, it is possible that the GroEL cross-links reflect "incidental" contacts away from the site(s) of direct chaperonin-Cdc10 interaction.

A homo-oligomeric group II chaperonin can partially replace *E. coli* GroEL; substitution at a single residue even allows it to restore growth to Δ*groEL*-mutant *E. coli* (Shah *et al.*, 2016). Nonetheless, GroEL and CCT bind actin very differently (Balchin *et al.*, 2018), and we want to be careful not to imply that the two chaperonins operate exactly the same way in septin folding. Septins may be among the proteins recently proposed to rely on CCT as a more GroEL-like "Anfinsen cage" that generally prevents aggregation and promotes native folding, without evolving a suite of specific contacts that establish client topology and direct a step-wise folding progression within the CCT chamber (Gestaut *et al.*, 2022). GroEL also works differently from DnaK, but each can support the folding of some clients in the absence of the other (Calloni *et al.*, 2012). The ability of Δ*dnaK* and other *E. coli* chaperone mutants to make septin octamers does not rule out roles for those chaperones in septin folding; other chaperones may compensate for their absence. Supplementing the PURExpress reactions with additional purified chaperones might further increase Cdc12 yield. Ultimately, a septin's path to the native conformation may look quite different depending on whether it passes through CCT or GroEL, even if the destination is the same. Finally, the ribosome itself acts as a chaperone to guide cotranslational protein folding (Cassaignau *et al.*, 2020), and we cannot exclude the possibility that differences between eukaryotic and prokaryotic ribosomes also create distinct folding trajectories with different chaperone requirements. Reconstituted eukaryotic cell–free translation systems to which purified chaperones can be added (Machida *et al.*, 2021) may be especially useful in this regard.

Our results and other published data are consistent with a model in which Cdc12 is translated more slowly than the other septins. Others have noted that while "programmed" slow translation, such

as by suboptimal codons, risks collision-induced mRNA and nascent protein degradation, it can also facilitate cotranslational folding and assembly by providing more time for interactions to occur (Collart and Weiss, 2020). If high ribosome density on Cdc12 mRNA reflects especially slow translation even in wild-type cells, it is tempting to speculate that Cdc12 acts as a platform for cotranslational septin assembly. Our previous studies (Weems and McMurray, 2017) support a model in which Cdc12 is the centerpiece for assembly of Cdc11/Shs1–Cdc12–Cdc3 trimers (Figure 7), which are subsequently brought together into hetero-octamers by a central Cdc10 homodimer. In this model, Cdc12 that has bound but not yet hydrolyzed GTP preferentially recruits Cdc11 (as opposed to Shs1) before interacting via its NC interface with Cdc3 (Weems and McMurray, 2017). Tubulins achieve a nearnative conformation within the CCT chamber that is capable of binding GTP (Tian *et al.*, 1995b; Gestaut *et al.*, 2022). If it is translated slowly enough, quasinative Cdc12•GTP might bind Cdc11 at its G interface and Cdc3 at its NC interface before ribosome release. The C-terminal ~90 residues of Cdc12 are dispensable for stable hetero-octamer assembly (Bertin *et al.*, 2010), so assembly could, in principle, be finished by the time Cdc12 translation is only ~80% complete.

Like Cdc12 compared with other yeast septins, different human septins may differ in their translation speeds and the effects of variation in chaperone activity. Variation in chaperone expression between different cell types can also drastically alter the ability of a protein to fold, as illustrated by the example of an oncogenic p53 mutant that misfolds in other cell types but folds and functions normally in embryonic stem cells, where CCT and other chaperones are more highly expressed and bind the mutant protein (Rivlin *et al.*, 2014). We previously showed how the presence of a "chemical chaperone," guanidine, alters Cdc3 folding to promote a septin assembly pathway that bypasses incorporation of Cdc10 (Johnson *et al.*, 2020). We think that our new findings point to cytosolic chaperones as key factors in dictating the landscape of septin complexes assembled in a given cell type.

MATERIALS AND METHODS

Request a protocol through *Bio-protocol*.

Detailed information about strains, plasmids, and oligonucleotides is provided in Supplemental Table 4.

Microbial cultivation

Yeast were cultured using standard methods (Amberg *et al.*, 2005) in liquid or solid (2% agar) rich medium (YPD; 1% yeast extract, 2% peptone, 2% glucose) or synthetic medium (SC; per liter, 20 g glucose, 1.7 g yeast nitrogen base without amino acids or ammonium sulfate, 5 g ammonium sulfate, 0.05 g tyrosine, 0.01 g arginine, 0.05 g aspartate, 0.05 g phenylalanine, 0.05 g proline, 0.05 g serine, 0.1 g threonine, 0.05 g valine, 0.05 g histidine, 0.1 g uracil, and 0.1 g leucine). Where appropriate to maintain plasmid selection, synthetic medium lacked specific components (uracil, tryptophan, histidine, etc.). Yeast were transformed using the Frozen-EZ Transformation II kit (Zymo Research #T2001). Bacteria were cultured in liquid or solid (1.5% agar) lysogeny broth (LB) medium (1% tryptone, 1% NaCl, 0.5% yeast extract) containing appropriate antibiotics and additives needed for plasmid selection and induction of gene expression. Unless otherwise stated, antibiotics and arabinose were used at the following final concentrations from 1000× stocks dissolved in water: carbenicillin at 70 µg/ml, ampicillin at 100 µg/ml, kanamycin at 40–50 µg/ml, chloramphenicol at 34 µg/ml (stock dissolved in ethanol), spectinomycin at 50 µg/ml, arabinose at 0.02%. *p*-Benzoyl-L-phenylalanine (Bpa;1 M) (Advanced Chemtech #YF2424) solution was freshly made before use by dissolving 27 mg of Bpa in 100 µl of 1 M NaOH. Bacterial transformation was performed using the Mix & Go! *E. coli* Transformation Kit (Zymo Research #T3001) or by making cells chemically competent using $CaCl_2$ (Sambrook and Russell, 2006).

Lysogenization and construction of *E. coli* chaperone deletion mutants

Lysogenization was accomplished with the λDE3 Lysogenization Kit (Novagen #69734 3). Host cells (1–2 µl) grown to mid–log phase at 37°C in LB containing 0.2% maltose and 10 mM $MgCl_2$ were combined with the three λ phages (10^8 CFU each), incubated at 37°C for 20 min, and spotted to LB. Several dozen to several hundred λDE3 lysogens were obtained following overnight growth at 37°C for strains BW25113, JW2573, and JW0462, which are from the "Keio" deletion collection (Baba *et al.*, 2006). Candidate lysogens were assayed with tester phage in top agarose (1% tryptone, 0.5% NaCl, 0.6% agarose), where plaques formed in the presence of 0.4 mM IPTG were slightly larger than those without IPTG. Lysogens were further confirmed by their immunity to selection phage and by visualization of a T7-driven GFP reporter (encoded by plasmid pDualeGFP; Supplemental Figure 11). Recombineering was accomplished using arabinose-induced expression of λ-red recombination genes from pSIJ8 (Jensen *et al.*, 2015) maintained in host cells before transformation with a *dnaJ*- or *dnaK*-targeting kanamycin resistance amplicon from strain JW0014 using dnaJ_keio_fw and dnaJ_keio-re or from strain JW0013 using dnaK_keio_fw and dnaK_keio_re. Bacteria were made chemically competent for recombineering using the Z-competent kit (Zymo Research #T3001) and recovered in super optimal broth with catabolite repression (SOC) at 30°C overnight before being plated on solid LB containing kanamycin at 30°C. The presence of the kanamycin resistance cassette insertion and the absence of duplicated wild-type allele were verified by PCR (Supplemental Figure 11). The temperature-sensitive loss of pSIJ8 was subsequently confirmed in recombinants. Note that host cells lacking DnaJ and DnaK cannot be lysogenized with λDE3 owing to the essential functions of those gene products in lambda phage replication. For this reason, Δ*dnaJ* and Δ*dnaK* were recombineered de novo in lysogen strain B002.

In vivo photocrosslinking

Yeast cells of the *upf1*Δ strain YRP2838 carrying pSNRtRNA-pBPA-RS (Krishnamurthy *et al.*, 2011) and a plasmid encoding a GST-6xHis–tagged septin were inoculated from single colonies into 5 ml of liquid synthetic medium lacking tryptophan and uracil and containing 2% raffinose. Septin expression plasmids were from a collection encoding GST-6xHis–tagged proteins (Zhu *et al.*, 2001) or mutant derivatives thereof. Following overnight growth at 30°C, the cultures were pelleted at 3500 × *g* for 5 min, washed once in fresh medium, and resuspended in a 250-ml baffled shaker flask at OD_{600} = 0.03 in 50 ml of fresh liquid synthetic medium lacking tryptophan and uracil and containing 2% raffinose. Cultures were grown shaking at 225 rpm and 30°C to OD_{600} = 0.5, at which point 50 µl of a 1 M solution of Bpa was added dropwise to the flask while swirling. Galactose was immediately added to 2% final concentration, and the cultures were rotated at 30°C for another 3 h. Cells were exposed, or not, to 254-nm light for 30 min in a Chromato-vue cabinet (Model C-70; Ultra-Violet Products) for 30 min in flat-bottom six-well dishes. Cultures were centrifuged at 4000 rpm, washed once with Equilibration Buffer A (300 mM NaCl, 50 mM Na_2PO_4, 50 mM Tris-HCl, pH 8.0, 0.05% octylphenoxy poly(ethyleneoxy)ethanol [Nonidet P-40 equivalent; Millipore-Sigma #i8896], 8 M urea) containing protease-inhibitor mix (Complete EDTA-free; Roche #11 873 580 001),

and frozen at –70°C. For detection of cross-linked species, cell pellets were resuspended in 400 µl of Equilibration Buffer A containing protease-inhibitor mix (Complete EDTA-free; Roche 11 873 580 001). Cells were lysed using the equivalent of 100 µl of glass beads and four cycles of 30-s on/off vortexing (incubating on ice during the "off" cycle). Samples were centrifuged at maximum speed to remove glass beads. Another 400 µl of Equilibration Buffer A was added to bead-free lysate and lysates were clarified by centrifugation at 12,000 × *g* at 4°C for 15 min. Clarified lysates were added to previously equilibrated His-Pur Ni-NTA spin columns (0.2 ml resin bed; Thermo Scientific #88224) and incubated at room temperature for 2 h. Flow-through ("Unbound") was transferred to another tube and columns washed twice, first with Equilibration Buffer A and second with Wash Buffer C (300 mM NaCl, 50 mM Na_2PO_4, 50 mM Tris-HCl, pH 8.0, 0.05% octylphenoxy poly(ethyleneoxy)ethanol, 8 M urea, 10 mM imidazole). His-tagged proteins ("Bound") were eluted in 200 µl of Elution Buffer B (300 mM NaCl, 50 mM Na_2PO_4, 50 mM Tris-HCl, pH 8.0, 0.05% octylphenoxy poly(ethyleneoxy)ethanol, 8 M urea, 250 mM imidazole).

For cross-linking in *E. coli*, single colonies of strain BL21(DE3) carrying plasmid pEVOL-pBpF (Chin *et al*., 2002) and a pET21-based Cdc10-encoding plasmid were used to inoculate 5-ml liquid cultures of LB with ampicillin and chloramphenicol. Following overnight growth at 37°C, the cultures were pelleted at 3500 × *g* for 5 min at room temperature, washed once in fresh LB with antibiotics, and resuspended in a 250-ml baffled shaker flask at an $OD_{600} = 0.03$ in 50 ml of fresh LB with antibiotics plus 0.02% arabinose to induce expression of the modified tRNA. Cultures were shaken at 37°C until the OD_{600} reached 0.5, at which point 50 µl of a 1 M solution of Bpa (made fresh by dissolving 27 mg in 100 µl of 1 M NaOH) was added dropwise to the flask while swirling. IPTG was immediately added to a 0.3 mM final concentration, and the cultures were shaken at 37°C for another 3 h. Cells were exposed, or not, to 254-nm light for 30 min as described above. Cultures were centrifuged at 4000 rpm, washed once with Equilibration Buffer B (300 mM NaCl, 20 mM Na_2PO_4, 8 M urea, 10 mM imidazole; pH 7.4) containing protease-inhibitor mix (Complete EDTA-free; Roche 11 873 580 001), and frozen at –70°C. For detection of cross-linked species, cell pellets were resuspended in 1 ml of Equilibration Buffer B containing protease-inhibitor mix (Complete EDTA-free; Roche 11 873 580 001) and 0.2 mg/ml lysozyme. Cells were incubated on ice for 15 min and subjected to two 15-s pulses of sonication (550 Sonic Dismembrator; Thermo Scientific) to complete lysis. Lysates were clarified by centrifugation at 12,000 × *g* at 4°C for 15 min. Clarified lysates were added to previously equilibrated His-Pur Ni-NTA spin columns (0.2 ml resin bed; Thermo Scientific #88224) and mixed end-over-end at 4°C for 30 min. Flow-through was discarded and columns washed twice with Wash Buffer D (300 mM NaCl, 20 mM Na_2PO_4, 8 M urea, 25 mM imidazole; pH 7.4). His-tagged proteins ("Bound") were eluted in 200 µl of Elution Buffer C (300 mM NaCl, 50 mM Na_2PO_4, 50 mM Tris-HCl, pH 8.0, 0.05% octylphenoxy poly(ethyleneoxy)ethanol, 8 M urea, 250 mM imidazole). Bound fractions were combined 1:1 with 2× SDS–PAGE sample buffer containing 10 mM dithiothreitol and heated at 95°C for 5 min before SDS–PAGE.

Heterologous coexpression of yeast septins

Cells carrying relevant plasmids described in the figure legends were inoculated from single colonies into 3-ml LB cultures with the indicated antibiotics and 0.02% arabinose (none for "No Septin Control"; ampicillin and chloramphenicol for B002, B003, B004, B005, and B006; ampicillin, chloramphenicol, and spectinomycin for strain 461). Cultures were grown overnight at 24°C and then pelleted and resuspended in fresh LB, after which 1–2 ml was inoculated in a 250-ml baffled shaker flask containing 200 ml of fresh LB with the indicated antibiotics and 0.02% arabinose. Cultures were shaken at 225 rpm and 24°C to $OD_{600} = 0.6$, after which 100 ml was removed and placed in a new flask and grown shaken at 37°C. Both 100-ml cultures were induced with 0.3 mM final IPTG, the original culture immediately at 24°C and the new culture following a 15-min acclimation period at 37°C. After 3 h cultures were centrifuged at 4000 rpm, washed once with Lysis Buffer B (300 mM NaCl, 2 mM $MgCl_2$, 1 mM EDTA, 5 mM β-mercaptoethanol, 0.5% Tween 20, 12% glycerol, 50 mM Tris-HCl, pH 8), and frozen at –70°C.

Expression and purification of individual yeast septins

6xHis-Cdc3 and Cdc12 were individually expressed in *E. coli* and purified by Keyclone Technologies. 6xHis-Cdc3 was produced using plasmid pBEG2 (Versele and Thorner, 2004). For Cdc12, a plasmid was constructed (pMBP-His-Cdc12) that fused to the N-terminus of Cdc12 maltose-binding protein (MBP), a heptahistidine (7xHis) tag, and a tobacco-etch mosaic virus (TEV) protease cleavage site. BL21(DE3) cells (300 ml) carrying the appropriate plasmid were induced at OD_{600} of 0.6 with 0.3 mM IPTG for 4 h at 32°C with shaking at 120 rpm. Cells were pelleted and lysed by sonication. The lysate was clarified by centrifugation, and the supernatant was loaded on a Ni-NTA column (Thermo Fisher Scientific) followed by washing and elution. The MBP-7xHis portion was cleaved using 6xHis-tagged TEV enzyme made by Keyclone Technologies, and the MBP-7xHis and 6xHis-TEV enzyme were removed by passage through the Ni-NTA column again after enzyme cleavage.

Mass spectrometry to identify yeast or *E. coli* proteins in cross-linking and in vitro translation experiments

Analysis was performed by the Mass Spectrometry Proteomics Shared Resource Facility of the University of Colorado Anschutz Medical Campus. Samples were processed with a filter-aided sample preparation (FASP) protocol (Wiśniewski, 2016). Briefly, aliquots containing 36 µg of total protein were mixed with 200 µl of 8 M urea in 0.1 M (ABC) ammonium bicarbonate (pH 8.5) reduced with 5 mM TCEP (tris(2-carboxyethyl)phosphine) for 20 min and alkylated with 50 mM 2-chloroacetamide for 15 min in the dark, all at room temperature. Reduced and alkylated samples were loaded onto 10-kDa-cutoff filters (Vivacon 500; Sartorius #VN01H02) and centrifuged at 14,000 × *g* for 20 min. The samples were then washed twice with 50 mM ABC and trypsin was added at an enzyme:protein ratio of 1:20 for overnight digestion at 37°C. Following trypsin digestion, samples were centrifuged at 14,000 × *g* for 20 min at room temperate and acidified with formic acid (FA) to a final concentration of 0.1%. Aliquots containing 10 µg of digested peptides were purified using Pierce C18 Spin Tips (Thermo Scientific #84850) according to the manufacturer's protocol, dried in a vacuum centrifuge, and resuspended in 0.1% FA in mass spectrometry–grade water. For cross-linking experiments, digested peptides were subjected to liquid chromatography mass spectrometry (LC-MS/MS) using an Eksigent nanoLC Ultra coupled to a LTQ-Orbitrap Velos Pro mass spectrometer. Fragmentation spectra were interpreted against the UniProt Fungi database using the Mascot search engine. One missed tryptic cleavage was allowed, and the precursor-ion mass tolerance and fragment-ion mass tolerance were set to 15 ppm and 0.6 Da, respectively. Carbamidomethyl (C) was selected as a fixed modification, and oxidation (M) was selected as a variable modification. The protein-level false discovery rate (FDR) was ≤ 1%. For in vitro translation experiments, LC-MS/MS was performed using an Easy nLC 1000 instrument coupled to a Q Exactive HF Mass Spectrometer

(both from Thermo Fisher Scientific). Peptides were loaded on a C18 column (100 µM inner diameter × 20 cm) packed in-house with 2.7 µm of Cortecs C18 resin and separated at a flow rate of 0.4 µl/min with solution A (0.1% FA) and solution B (0.1% FA in acetonitrile) and under the following conditions: isocratic at 4% B for 3 min, followed by 4–32% B for 102 min, 32–55% B for 5 min, 55–95% B for 1 min, and isocratic at 95% B for 9 min. The mass spectrometer was operated in data-dependent acquisition (DDA) mode with the top 15 most abundant precursors being selected for MS/MS analysis. Fragmentation spectra were searched against the UniProt Escherichia coli proteome database combined with the Cdc10 and Cdc12 protein sequences using the MSFragger-based FragPipe computational platform (Kong *et al.*, 2017). Contaminants and reverse decoys were added to the database automatically. The precursor-ion mass tolerance and fragment-ion mass tolerance were set to 10 ppm and 0.2 Da, respectively. Fixed modifications were set as carbamidomethyl (C), and oxidation (M) was selected as a variable modification. Two missed tryptic cleavages were allowed, and the protein-level FDR was ≤1%.

Hydrogen-deuterium exchange mass spectrometry

HDX-MS was performed at the University of Colorado, Boulder, Central Analytical Mass Spectrometry lab. To identify peptic fragments of Cdc3, 100 pmoles of protein (5 µl) was mixed with 45 µl of the sample buffer (150 mM NaCl, 25 mM HEPES, 5% glycerol, pH 7.4) and then mixed with 50 µl of a quenching buffer (3 M guanidine HCl, 1.5% formic acid). The whole sample (100 µl total) was injected into a Waters HDX-LC box in which protein was digested by an online pepsin column (Waters Enzymate BEH pepsin column, 2.1 × 30 mm, 5 µm, and the resulting peptic peptides were trapped and desalted on a Waters ACQUITY UPLC BEH C4 1.7 µm VanGuard Pre-column (2.1 × 5 mm) at 100 µl/min Buffer A (0.1% formic acid in water) for 3 min. The digestion chamber was kept at 15°C, and the trap and analytical columns were at 0°C. The peptides were eluted with 3–33% Buffer B (0.1% formic acid in acetonitrile) between 0 and 6 min, 33–40% B between 6 and 6.5 min, and 40–85% B between 6.5 and 7 min. The eluted peptides were resolved on a Waters ACQUITY UPLC Protein BEH C4 column (300 Å, 1.7 µm, 1 mm × 50 mm). MS/MS spectra were performed on a Thermo LTQ orbitrap Velos mass spectrometer. The peptides were ionized using electrospray ionization (ESI) with the source voltage = 5.0 kV and S-lens RF level = 60%. The capillary temperature was 275°C, and the source heater was off. The sheath gas flow was 10. Precursor ions were scanned between 350 and 1800 m/z at 60,000 resolution with AGC 1×10^6 (max ion fill time = 500 ms). From the precursor scan, the top 10 most intense ions were selected for MS/MS with 180 s dynamic exclusion (10 ppm exclusion window, repeat count = 1) and AGC 1×10^4 (max ion fill time = 100 ms). Ions with unassigned charge states were rejected for MS/MS. The normalized collision energy was 35%, with activation Q = 0.25 for 10 ms. MS/MS spectra were searched against a database consisting of Cdc3 protein sequence in a FASTA format using the MaxQuant/Andromeda program (version 1.6.3.4) developed by the Cox lab at the Max Planck Institute of Biochemistry (Cox and Mann, 2008; Cox *et al.*, 2011). The digestion mode was "unspecific," and oxidation of methionine was set as a variable modification. The minimum peptide length for the unspecific search was 8. MaxQuant/Andromeda used 4.5 ppm for the main search peptide tolerance and 0.5 Da for MS/MS tolerance. The FDR was 0.01. A list of peptides identified from the search was used as an exclusion list for the next round of LC-MS/MS, and a total of three LC-MS/MS were performed for each protein.

For hydrogen-deuterium exchange, 10 250 µl aliquots of the sample buffer were dried using vacuum centrifugation, reconstituted with an equal volume of deuterium oxide ("D_2O buffer"), and put in a 10°C water bath. Ten minutes before the initiation of the HDX reaction, 5 µl of Cdc3 protein (100 pmoles) was transferred to a 0.5 ml tube and incubated at 10°C. The HDX reaction was initiated by the addition of the D_2O buffer (45 µl) to the 10 µl sample (90% D_2O final). The reaction was quenched at 15 s, 30 s, 1 min, 2 min, 5 min, 10 min, 20 min, 40 min, 80 min, and 120 min after the initiation by the addition of the quench buffer (50 µl). The whole sample (100 µl) was injected into the Waters HDX-LC box, and LC-MS was performed as described above. For HDX samples, only MS1 spectra were recorded. For the 0 s control, 100 pmoles of Cdc3 (5 µl) was mixed with 50 µl of the quenching solution and then with 45 µl of the D_2O buffer. HDX-MS data were analyzed using Mass Spec Studio (version 2.4.0.3484) developed by the Schriemer lab at the University of Calgary (Rey *et al.*, 2014; Raval *et al.*, 2021). "Peptide.txt" and "evidence.txt" from the MaxQuant/Andromeda search results were used to generate the "identification" table for Mass Spec Studio using an in-house Python script. The raw files from the Thermo LTQ orbitrap Velos were converted to mzML files using ProteoWizard (version 3.0.20216, 64 bit). The default processing parameters were used except mass tolerance = 15 ppm, total retention time width = 0.15 min, XIC smoothing = Savitzky Golay Smoothing, and deconvolution method = centroid. All processed data were manually validated.

Exchange ratio values were mapped onto the AlphaFold2-predicted Cdc3 structure using the "spectrum b" function in the PyMOL Molecular Graphics System v2.0 (Schrödinger, LLC). Briefly, the .pdb file was edited to replace the B values with average exchange ratios at 120 min. Residues not detected by mass spectrometry were assigned an exchange value of 2, and the structure rendered in PyMol was colored using the command "spectrum b, blue red grey, minimum = 0, maximum = 2."

ATPase and refolding activity of purified GroEL/ES

GroES and GroEL were obtained from the Takara Biotechnology (Dalian) Co., Ltd (#7331 and #7330). ATPase activity was measured using the EnzChek Phosphate Assay Kit (Thermo Fisher Scientific #E6646) according to the manufacturer's instructions with 500 nM GroEL/ES tetradecamer. Rhodanese refolding was monitored as absorbance at 460 nm in a 96-well plate using the same device. Rhodanese (Sigma #R1756-5MG) was denatured in 8 M urea. The thiocyanate enzymatic assay stock was 140 mM KH_2PO_4, 160 mM KCN (Sigma-Aldrich #207810), and 160 mM $Na_2S_2O_3$ in water. Reagent concentrations during refolding reactions were 300 nM GroEL, 360 nM GroES, 250 nM denatured rhodanese, 1 mM ATP. The formaldehyde quench stock was 30% formaldehyde in water. The ferric nitrate reporter stock was 8.5% wt/vol $Fe(NO_3)_3$ and 11.3% vol/vol HNO_3 in water. Absorbance at 360 nm was measured after 15 min with a 96-well plate using a plate reader (Cytation 3; BioTek).

In vitro translation

The PURExpress ΔRF123 kit (New England Biolabs #E6850S) was used with the following modifications from the manufacturer's instructions. As described previously (Kawahashi *et al.*, 2007), fluorescent puromycin (6-FAM-dC-puromycin; Jena Bioscience #NU-925-6FM-L) was added to 4.6 µM. Purified EF-P was purchased from Biomatik (#RPC22718) and, as described in Ude *et al.* (2013), was added to 1 µM where indicated, or a control buffer (20 mM Tris-HCl, pH 8.0, 0.5 M NaCl, 6% trehalose) was added. Purified GroES and GroEL were each added to 0.87 µM where indicated, or a control

buffer (50 mM Tris-HCl, pH 7.4, 50 mM KCl, 10 mM $MgCl_2$) was added. Additional ATP was added to 6.7 mM (not including ATP included in PURExpress kit reagents) to prevent ATP depletion resulting from added GroEL/ES. Template plasmid (pMVB128) (62 ng) was added to each reaction, and 16 U of RNase inhibitor was included. Per the manufacturer's instructions, the reactions were completed at 37°C, and the total reaction time was 3 h. Completed reactions were analyzed immediately or stored at –20°C.

Analysis of purified septin oligomerization state

Purified Adh1 (Sigma-Aldrich #A8656-1VL) or Cdc3 were diluted in phosphate-buffered saline (PBS) and centrifuged through 0.5 ml 100-kDa-molecular-weight cutoff protein concentrators (Thermo Scientific Pierce #PI88503) according to the manufacturer's instructions. Analytical SEC was performed with an Agilent AdvanceBio SEC 300Å 2.7 µm w/Guard Column equilibrated and run at 0.3 ml/min in PBS with GTP (Sigma-Aldrich #51120) or guanidine added as indicated. Protein was injected in 50 µl. Molecular weight standards were AdvanceBio SEC 300Å Protein Standard (#5190-9417).

SDS–PAGE and immunoblotting

Where indicated in figure legends, proteins were extracted from yeast cells using an alkaline lysis/trichloroacetic acid (TCA) precipitation method (Hase *et al.*, 1983). Proteins were typically resolved on 10% SDS–PAGE gels. Immunoblotting was performed via semi-dry transfer (Bio-Rad #1703940) to polyvinylidene fluoride membranes. Primary antibodies were anti-GroEL (Enzo Life Sciences #ADI-SPS-870-D, RRID:AB_2039163), anti-DnaK (Enzo Life Sciences #ADI-SPA-880-F, RRID:AB_10619012), anti-GST (Santa Cruz Biotechnology #sc-459, RRID:AB_631586), anti-6xHis (UBPBio #Y1011), anti-Cdc11 (Santa Cruz Biotechnology #sc-7170, RRID:AB_671797), anti-Cdc3 (McMurray and Thorner, 2008). Secondary antibodies were infrared-labeled anti-mouse (680 nm; Biotium #20061-1, RRID:AB_10854088), infrared-labeled anti-rabbit (800 nm; Cell Signaling Technology #5151, RRID:AB_10697505). Immunoblots were scanned on a Li-Cor Odyssey. Gels with fluorescent puromycin were scanned on a Sapphire Biomolecular Imager (Azure Biosystems).

In vivo assays of kinetics of septin folding and posttranslational assembly

All experiments were carried out at room temperature (~22°C). With a few exceptions, noted below and in the figure legends, cells were BY4741 (haploid wild-type parent strain) or BY4743 (diploid wild-type parent strain) or derivatives thereof carrying the plasmid(s) pTS395 (*URA3* P_{GAL}*–GFP*) (Carminati and Stearns, 1997), pMVB1 (*URA3* P_{GAL}*–CDC3-GFP*) (Schaefer *et al.*, 2016), pMVB2 (*URA3* P_{GAL}*–CDC12-GFP*) (Versele *et al.*, 2004), pMVB3 (*URA3* P_{GAL}*–CDC11-GFP*), YEpPgal–GST-His6-Cdc12 (*URA3* P_{GAL}*–GST-5xHis-CDC12*) (Zhu *et al.*, 2001), and/or pGF-IVL-470 (*URA3* P_{GAL}*–CDC12-mCherry*). The *cct4* and *cdc3(G365R)* strains were from a BY4741-based temperature-sensitive mutant collection (Li *et al.*, 2011). The *ssb1*Δ, *hsc82*Δ, and *hsp82*Δ strains were from the deletion collection made in BY4741 (Winzeler *et al.*, 1999). The *ssa1*Δ and *ssa4*Δ strains were from the deletion collection made in BY4742 (*MAT his3*Δ *leu2*Δ *lys2*Δ *ura3*Δ) (Winzeler *et al.*, 1999). Cells containing plasmids were cultured to mid–log phase in synthetic complete media lacking uracil, leucine, and/or tryptophan and containing 2% raffinose or sodium lactate, which neither induces nor represses the *GAL1/10* promoter.

The kinetics-of-folding experiment in *cct4* cells and the corresponding wild-type control experiment were performed by loading cells into an ONIX EV-262 Microfluidic Perfusion Platform (CellAsic #NX-262, plate #Y04C). Galactose-containing medium was flowed into the chamber, and flow was maintained at a constant rate thereafter. To avoid phototoxicity, different cells were visualized at each time point after galactose addition, with the exception of several fields of cells that were imaged by transmitted light both at time 0 and after 13.5 h for the purpose of retrospectively assessing relative division rate. For other kinetics-of-folding experiments, galactose was added at "time 0" to 0.05% or 0.1% final concentration to liquid raffinose or lactate cultures, and aliquots were removed at each time point and spotted onto agarose pads for microscopy. For the kinetics of Cdc11-GFP and Cdc12-mCherry, we improved our analysis by blinding the investigator to the identity of each sample before quantification and analyzing only cells with cytoplasmic/nuclear intensity under a maximum threshold value (10,000 a.u. for *ssb1*Δ, 6000 a.u. for *cct4-1*), allowing more uniform comparison between chaperone mutants and their wild-type control. Threshold values were determined by the maximum cytoplasmic intensity for which septin ring intensity measurements could be accurately measured, above which the cytoplasmic/nuclear signal was too bright to observe septin ring–specific fluorescence. We also used septin ring maximum intensity values, without subtracting surrounding background signal from the cytoplasm, because we measured and plotted the cytoplasmic/nuclear signal separately. For posttranslational assembly experiments, expression was terminated after 6 h of induction by transferring cells to fresh medium containing 2% glucose. Aliquots of cells from glucose cultures were imaged at various time points, and the number of cell divisions since the previous time point was calculated using a hemacytometer. Cultures were occasionally backdiluted into fresh media to prevent culture saturation, and cultures were temporarily stored overnight at 4°C as necessary throughout the data collection period.

RT-PCR

Culture (500 µl) was preserved and pelleted with RNAprotect Bacteria Reagent (Qiagen #76506) before freezing at –70°C. Cell pellets were thawed and lysed in 200 µl of TE (10 mM Tris-HCl, 1 mM EDTA, pH 8) buffer containing 20 mg total Proteinase K and 15 mg/ml lysozyme. RNA was isolated from bacterial lysate using the RNeasy Mini kit (Qiagen #74104) and eluted in sterile RNase-free water. RNA samples were quantified by Nanodrop and treated with TURBO DNase (Thermo Scientific Invitrogen #AM1907). DNase-treated RNA (≤500 ng) was used to generate cDNA using Protoscript II Reverse Transcriptase (New England Biolabs #M0368) and the standard first-strand cDNA synthesis protocol. Reverse transcriptase (RT)-PCR with OneTaq (New England Biolabs #M0480S) was performed on cDNA preparations, typically using 0.25–0.5 µl cDNA input in a 25-µl reaction with 25 cycles. Annealing temperature and extension time were 53°C and 50 s for Cdc12 and 51°C and 60 s for Cdc3.

Microscopy

Images were captured with an EVOSfl all-in-one epifluorescence microscope (Thermo Fisher Scientific) with a 60× oil objective and GFP (#AMEP4651) and Texas Red (#AMEP4655) LED/filter cubes. Image adjustment and analysis was carried out using FIJI software (Schindelin *et al.*, 2012). Septin ring fluorescence was assessed with line scans (width 8 pixels) perpendicularly across septin rings measuring the difference between maximum and minimum pixel intensity values, except for some experiments where the maximum values were used directly, as indicated above. The integrated pixel intensity inside an 8- or 10-pixel-diameter circle was used to

approximate the cytoplasmic/nuclear fluorescent signal for each cell (vacuoles were avoided when possible). A minimum of 30 cells were analyzed at each time point.

In vivo imaging of septin foci resulting from overexpression

JTY3992 (McMurray *et al.*, 2011a) is derived from BY4742 with mCherry fused to the C-terminus of Cdc10. The *HSP104-mCherry* strain was made by homologous recombination using a donor PCR product made with template plasmid pDK305 (Kaganovich *et al.*, 2008) and primers GFPtomCherryfw and GFPtomCherryre70, co-transformed with plasmid pGF-V2226 (Roggenkamp *et al.*, 2017) into cells of the *HSP104-GFP* strain from the BY4741-based GFP collection (Huh *et al.*, 2003) that were already carrying plasmid pML104 (Laughery *et al.*, 2015). Cas9-mediated cutting of the GFP sequence was repaired by homologous recombination with the mCherry-encoding PCR product, replacing the GFP and the downstream *HIS3MX* marker. The Cdc3-mCherry strain was made by integrating *Bgl*II-digested plasmid yIp128-Cdc3-mcherry (Tong *et al.*, 2007) into BY4743. Chaperone deletion strains were from the BY4742-based haploid or BY4743-based homozygous diploid deletion collections (Winzeler *et al.*, 1999). Cdc12-GFP foci were induced by culturing cells carrying pMVB2 in synthetic medium with 2% galactose at room temperature. Cdc12-mCherry was overexpressed in the same way using plasmid pGF-IVL-470. Cdc10(Asp182Asn)-GFP foci were induced by culturing cells carrying pPmet-cdc10-1-GFP in synthetic medium lacking methionine (to induce the *MET15* promoter) at room temperature or shifted to 37°C for 6 h. For analysis of Cdc12-GFP focus appearance and disappearance in *hsp104*Δ mutants, synthetic cultures grown in 2% raffinose overnight were diluted into 25 ml of fresh medium with 0.1% galactose and 1.9% raffinose. After 6 h of induction, the cells were pelleted and resuspended in synthetic medium with 2% glucose.

Predicted protein structures

AlphaFold-predicted protein structures were accessed from the AlphaFold Protein Structure Database (Jumper *et al.*, 2021; Varadi *et al.*, 2022) at the following entries: Cdc3 (P32457), Cdc11 (P32458), Cdc12 (P32468), Ssa1 (P10591), Ssa2 (P10592), Ydj1 (P25491), and Zuo1 (P32527). Structures were imaged in PyMOL (Schrödinger LLC).

Analysis of Cdc3 and Cdc12 sequences for potential translation-slowing properties

Data for the codon adaptation index (CAI) for the Cdc3 and Cdc12 coding sequences were obtained from the Codon Usage Database (https://www.kazusa.or.jp/codon/) for yeast (species 4932) and *E. coli* (species 83333) (Nakamura *et al.*, 2000). For predicted mRNA secondary structures, the coding sequences were analyzed at the mFold RNA server (http://www.unafold.org/mfold/applications/rna-folding-form.php) (Zuker, 2003) using default settings/parameters. For amino acid pairs, each pair of amino acids in the Cdc3 and Cdc12 sequences was assessed according to published semiquantitative bins of effect on translation elongation speed (Ahmed *et al.*, 2020) and color-coded using a custom macro in Microsoft Excel.

ACKNOWLEDGMENTS

We thank Corrine Tuckey of New England Biolabs for insights and advice with PURExpress reactions; Thomas Lee of the Boulder Central Analytical Mass Spectrometry lab for carrying out the HDX-MS analysis; Monika Dzieciatkowska and Anthony Saviola of the Proteomics Mass Spec Facility for their MS analysis; Jun Yang of Keyclone Technologies for mutagenesis, cloning, and protein expression and purification; Kevin Stein of the Frydman lab at Stanford University for sharing unpublished results about cotranslational interactions between chaperones and septins; and Greg Finnigan of Kansas State University for sharing unpublished septin and CRISPR plasmids. The work was supported by the National Institute of General Medical Sciences of the National Institutes of Health under Award no. R01GM124024 (to M. M.) and Award no. T32GM008730 (to A. D).

REFERENCES

Abbey M, Hakim C, Anand R, Lafera J, Schambach A, Kispert A, Taft MH, Kaever V, Kotlyarov A, Gaestel M, *et al.* (2016). GTPase domain driven dimerization of SEPT7 is dispensable for the critical role of septins in fibroblast cytokinesis. Sci Rep 6, 20007.

Ahmed N, Friedrich UA, Sormanni P, Ciryam P, Altman NS, Bukau B, Kramer G, O'Brien EP (2020). Pairs of amino acids at the P- and A-sites of the ribosome predictably and causally modulate translation-elongation rates. J Mol Biol 432, 166696.

Alamgir M, Erukova V, Jessulat M, Azizi A, Golshani A (2010). Chemical-genetic profile analysis of five inhibitory compounds in yeast. BMC Chem Biol 10, 6.

Albanèse V, Yam AY-W, Baughman J, Parnot C, Frydman J (2006). Systems analyses reveal two chaperone networks with distinct functions in eukaryotic cells. Cell 124, 75–88.

Amberg D, Burke D, Strathern J (2005). Methods in Yeast Genetics: A Cold Spring Harbor Laboratory Course Manual, 2005 ed, Cold Spring Harbor, NY: Cold Spring Harbor Laboratory Press.

Arava Y, Wang Y, Storey JD, Liu CL, Brown PO, Herschlag D (2003). Genome-wide analysis of mRNA translation profiles in Saccharomyces cerevisiae. Proc Natl Acad Sci USA 100, 3889–3894.

Baba T, Ara T, Hasegawa M, Takai Y, Okumura Y, Baba M, Datsenko KA, Tomita M, Wanner BL, Mori H (2006). Construction of Escherichia coli K-12 in-frame, single-gene knockout mutants: the Keio collection. Mol Syst Biol 2, 2006.0008.

Balchin D, Hayer-Hartl M, Hartl FU (2016). In vivo aspects of protein folding and quality control. Science 353, aac4354.

Balchin D, Miličić G, Strauss M, Hayer-Hartl M, Hartl FU (2018). Pathway of actin folding directed by the eukaryotic chaperonin TRiC. Cell 174, 1507–1521.e16.

Bertin A, McMurray MA, Grob P, Park S-S, Garcia G, Patanwala I, Ng H-L, Alber T, Thorner J, Nogales E (2008). Saccharomyces cerevisiae septins: supramolecular organization of heterooligomers and the mechanism of filament assembly. Proc Natl Acad Sci USA 105, 8274–8279.

Bertin A, McMurray MA, Thai L, Garcia G, Votin V, Grob P, Allyn T, Thorner J, Nogales E (2010). Phosphatidylinositol-4,5-bisphosphate promotes budding yeast septin filament assembly and organization. J Mol Biol 404, 711–731.

Boël G, Letso R, Neely H, Price WN, Wong K-H, Su M, Luff J, Valecha M, Everett JK, Acton TB, *et al.* (2016). Codon influence on protein expression in E. coli correlates with mRNA levels. Nature 529, 358–363.

Bolanos-Garcia VM, Davies OR (2006). Structural analysis and classification of native proteins from E. coli commonly co-purified by immobilised metal affinity chromatography. Biochim Biophys Acta 1760, 1304–1313.

Brausemann A, Gerhardt S, Schott A-K, Einsle O, Große-Berkenbusch A, Johnsson N, Gronemeyer T (2016). Crystal structure of Cdc11, a septin subunit from Saccharomyces cerevisiae. J Struct Biol 193, 157–161.

Bridges AA, Zhang H, Mehta SB, Occhipinti P, Tani T, Gladfelter AS (2014). Septin assemblies form by diffusion-driven annealing on membranes. Proc Natl Acad Sci USA 111, 2146–2151.

Brownridge P, Lawless C, Payapilly AB, Lanthaler K, Holman SW, Harman VM, Grant CM, Beynon RJ, Hubbard SJ (2013). Quantitative analysis of chaperone network throughput in budding yeast. Proteomics 13, 1276–1291.

Burkhardt DH, Rouskin S, Zhang Y, Li G-W, Weissman JS, Gross CA (2017). Operon mRNAs are organized into ORF-centric structures that predict translation efficiency. eLife 6, e22037.

Calloni G, Chen T, Schermann SM, Chang H-C, Genevaux P, Agostini F, Tartaglia GG, Hayer-Hartl M, Hartl FU (2012). DnaK functions as a central hub in the E. coli chaperone network. Cell Rep 1, 251–264.

Carminati JL, Stearns T (1997). Microtubules orient the mitotic spindle in yeast through dynein-dependent interactions with the cell cortex. J Cell Biol 138, 629–641.

Cassaignau AME, Cabrita LD, Christodoulou J (2020). How does the ribosome fold the proteome? Annu Rev Biochem 89, 389–415.
Chapman E, Farr GW, Usaite R, Furtak K, Fenton WA, Chaudhuri TK, Hondorp ER, Matthews RG, Wolf SG, Yates JR, *et al.* (2006). Global aggregation of newly translated proteins in an Escherichia coli strain deficient of the chaperonin GroEL. Proc Natl Acad Sci USA 103, 15800–15805.
Charneski CA, Hurst LD (2013). Positively charged residues are the major determinants of ribosomal velocity. PLoS Biol 11, e1001508.
Chen L, Sigler PB (1999). The crystal structure of a GroEL/peptide complex: plasticity as a basis for substrate diversity. Cell 99, 757–768.
Chen Y, Tsai B, Li N, Gao N (2022). Structural remodeling of ribosome associated Hsp40-Hsp70 chaperones during co-translational folding. Nat Commun 13, 3410.
Chin JW, Martin AB, King DS, Wang L, Schultz PG (2002). Addition of a photocrosslinking amino acid to the genetic code of Escherichia coli. Proc Natl Acad Sci USA 99, 11020–11024.
Collart MA, Weiss B (2020). Ribosome pausing, a dangerous necessity for co-translational events. Nucleic Acids Res 48, 1043–1055.
Costanzo M, Baryshnikova A, Bellay J, Kim Y, Spear ED, Sevier CS, Ding H, Koh JLY, Toufighi K, Mostafavi S, *et al.* (2010). The genetic landscape of a cell. Science 327, 425–431.
Costanzo M, VanderSluis B, Koch EN, Baryshnikova A, Pons C, Tan G, Wang W, Usaj M, Hanchard J, Lee SD, *et al.* (2016). A global genetic interaction network maps a wiring diagram of cellular function. Science 353, aaf1420.
Cox J, Mann M (2008). MaxQuant enables high peptide identification rates, individualized p.p.b.-range mass accuracies and proteome-wide protein quantification. Nat Biotechnol 26, 1367–1372.
Cox J, Neuhauser N, Michalski A, Scheltema RA, Olsen JV, Mann M (2011). Andromeda: a peptide search engine integrated into the MaxQuant environment. J Proteome Res 10, 1794–1805.
Dekker C, Stirling PC, McCormack EA, Filmore H, Paul A, Brost RL, Costanzo M, Boone C, Leroux MR, Willison KR (2008). The interaction network of the chaperonin CCT. EMBO J 27, 1827–1839.
Denney AS, Weems AD, McMurray MA (2021). Selective functional inhibition of a tumor-derived p53 mutant by cytosolic chaperones identified using split-YFP in budding yeast. G3 Genes/Genomics/Genetics 11, jkab230.
Dombek KM, Kacherovsky N, Young ET (2004). The Reg1-interacting proteins, Bmh1, Bmh2, Ssb1, and Ssb2, have roles in maintaining glucose repression in Saccharomyces cerevisiae. J Biol Chem 279, 39165–39174.
Dunn CD, Jensen RE (2003). Suppression of a defect in mitochondrial protein import identifies cytosolic proteins required for viability of yeast cells lacking mitochondrial DNA. Genetics 165, 35–45.
Farkasovsky M, Herter P, Voss B, Wittinghofer A (2005). Nucleotide binding and filament assembly of recombinant yeast septin complexes. Biol Chem 386, 643–656.
Fernandez-Escamilla A-M, Rousseau F, Schymkowitz J, Serrano L (2004). Prediction of sequence-dependent and mutational effects on the aggregation of peptides and proteins. Nat Biotechnol 22, 1302–1306.
Frazier JA, Wong ML, Longtine MS, Pringle JR, Mann M, Mitchison TJ, Field C (1998). Polymerization of purified yeast septins: evidence that organized filament arrays may not be required for septin function. J Cell Biol 143, 737–749.
Fredrick K, Ibba M (2010). How the sequence of a gene can tune its translation. Cell 141, 227–229.
Gamble CE, Brule CE, Dean KM, Fields S, Grayhack EJ (2016). Adjacent codons act in concert to modulate translation efficiency in yeast. Cell 166, 679–690.
Gao Y, Vainberg IE, Chow RL, Cowan NJ (1993). Two cofactors and cytoplasmic chaperonin are required for the folding of alpha- and beta-tubulin. Mol Cell Biol 13, 2478–2485.
Garcia G 3rd, Bertin A, Li Z, Song Y, McMurray MA, Thorner J, Nogales E (2011). Subunit-dependent modulation of septin assembly: budding yeast septin Shs1 promotes ring and gauze formation. J Cell Biol 195, 993–1004.
Gestaut D, Limatola A, Joachimiak L, Frydman J (2019). The ATP-powered gymnastics of TRiC/CCT: an asymmetric protein folding machine with a symmetric origin story. Curr Opin Struct Biol 55, 50–58.
Gestaut DR, Zhao Y, Park J, Ma B, Leitner A, Collier M, Pintilie G, Roh SH, Chiu W, Frydman J (2022). Structural visualization of the tubulin folding pathway directed by eukaryotic chaperonin TRiC. BioRxiv 2022.03.25.483853.
Goldberg AL (2003). Protein degradation and protection against misfolded or damaged proteins. Nature 426, 895–899.
Goldberg AL, Dice JF (1974). Intracellular protein degradation in mammalian and bacterial cells. Annu Rev Biochem 43, 835–869.
Goldman DH, Kaiser CM, Milin A, Righini M, Tinoco I, Bustamante C (2015). Mechanical force releases nascent chain-mediated ribosome arrest in vitro and in vivo. Science 348, 457–460.
Goloubinoff P, Christeller JT, Gatenby AA, Lorimer GH (1989a). Reconstitution of active dimeric ribulose bisphosphate carboxylase from an unfoleded state depends on two chaperonin proteins and Mg-ATP. Nature 342, 884–889.
Goloubinoff P, Gatenby AA, Lorimer GH (1989b). GroE heat-shock proteins promote assembly of foreign prokaryotic ribulose bisphosphate carboxylase oligomers in Escherichia coli. Nature 337, 44–47.
Hartwell LH (1971). Genetic control of the cell division cycle in yeast. IV. Genes controlling bud emergence and cytokinesis. Exp Cell Res 69, 265–276.
Hase T, Riezman H, Suda K, Schatz G (1983). Import of proteins into mitochondria: nucleotide sequence of the gene for a 70-kd protein of the yeast mitochondrial outer membrane. EMBO J 2, 2169–2172.
Hasin N, Cusack SA, Ali SS, Fitzpatrick DA, Jones GW (2014). Global transcript and phenotypic analysis of yeast cells expressing Ssa1, Ssa2, Ssa3 or Ssa4 as sole source of cytosolic Hsp70-Ssa chaperone activity. BMC Genomics 15, 194.
Haslbeck M, Braun N, Stromer T, Richter B, Model N, Weinkauf S, Buchner J (2004). Hsp42 is the general small heat shock protein in the cytosol of Saccharomyces cerevisiae. EMBO J 23, 638–649.
Hayer-Hartl M, Bracher A, Hartl FU (2016). The GroEL-GroES chaperonin machine: a nano-cage for protein folding. Trends Biochem Sci 41, 62–76.
Horwich AL, Low KB, Fenton WA, Hirshfield IN, Furtak K (1993). Folding in vivo of bacterial cytoplasmic proteins: role of GroEL. Cell 74, 909–917.
Hübscher V, Mudholkar K, Chiabudini M, Fitzke E, Wölfle T, Pfeifer D, Drepper F, Warscheid B, Rospert S (2016). The Hsp70 homolog Ssb and the 14-3-3 protein Bmh1 jointly regulate transcription of glucose repressed genes in Saccharomyces cerevisiae. Nucleic Acids Res. 44, 5629–5645.
Huh W-K, Falvo JV, Gerke LC, Carroll AS, Howson RW, Weissman JS, O'Shea EK (2003). Global analysis of protein localization in budding yeast. Nature 425, 686–691.
Jensen SI, Lennen RM, Herrgård MJ, Nielsen AT (2015). Seven gene deletions in seven days: fast generation of Escherichia coli strains tolerant to acetate and osmotic stress. Sci Rep 5, 17874.
Joachimiak LA, Walzthoeni T, Liu CW, Aebersold R, Frydman J (2014). The structural basis of substrate recognition by the eukaryotic chaperonin TRiC/CCT. Cell 159, 1042–1055.
Johnson CR, Steingesser MG, Weems AD, Khan A, Gladfelter A, Bertin A, McMurray MA (2020). Guanidine hydrochloride reactivates an ancient septin hetero-oligomer assembly pathway in budding yeast. eLife 9, e54355.
Johnson CR, Weems AD, Brewer JM, Thorner J, McMurray MA (2015). Cytosolic chaperones mediate quality control of higher-order septin assembly in budding yeast. Mol Biol Cell 26, 1323–1344.
Jores T, Lawatscheck J, Beke V, Franz-Wachtel M, Yunoki K, Fitzgerald JC, Macek B, Endo T, Kalbacher H, Buchner J, *et al.* (2018). Cytosolic Hsp70 and Hsp40 chaperones enable the biogenesis of mitochondrial β-barrel proteins. J Cell Biol 217, 3091–3108.
Jumper J, Evans R, Pritzel A, Green T, Figurnov M, Ronneberger O, Tunyasuvunakool K, Bates R, Žídek A, Potapenko A, *et al.* (2021). Highly accurate protein structure prediction with AlphaFold. Nature 596, 583–589.
Kaganovich D, Kopito R, Frydman J (2008). Misfolded proteins partition between two distinct quality control compartments. Nature 454, 1088–1095.
Kawahashi Y, Doi N, Oishi Y, Tsuda C, Takashima H, Baba T, Mori H, Ito T, Yanagawa H (2007). High-throughput fluorescence labelling of full-length cDNA products based on a reconstituted translation system. J Biochem 141, 19–24.
Kerner MJ, Naylor DJ, Ishihama Y, Maier T, Chang H-C, Stines AP, Georgopoulos C, Frishman D, Hayer-Hartl M, Mann M, *et al.* (2005). Proteome-wide analysis of chaperonin-dependent protein folding in Escherichia coli. Cell 122, 209–220.
Kim S, Schilke B, Craig EA, Horwich AL (1998). Folding in vivo of a newly translated yeast cytosolic enzyme is mediated by the SSA class of cytosolic yeast Hsp70 proteins. Proc Natl Acad Sci USA 95, 12860–12865.
Knowlton JJ, Gestaut D, Ma B, Taylor G, Seven AB, Leitner A, Wilson GJ, Shanker S, Yates NA, Prasad BVV, *et al.* (2021). Structural and functional

dissection of reovirus capsid folding and assembly by the prefoldin-TRiC/CCT chaperone network. Proc Natl Acad Sci USA 118, e2018127118.
Kong AT, Leprevost FV, Avtonomov DM, Mellacheruvu D, Nesvizhskii AI (2017). MSFragger: ultrafast and comprehensive peptide identification in mass spectrometry-based proteomics. Nat Methods 14, 513–520.
Kota P, Summers DW, Ren H-Y, Cyr DM, Dokholyan NV (2009). Identification of a consensus motif in substrates bound by a type I Hsp40. Proc Natl Acad Sci USA 106, 11073–11078.
Krishnamurthy M, Dugan A, Nwokoye A, Fung Y-H, Lancia JK, Majmudar CY, Mapp AK (2011). Caught in the act: covalent cross-linking captures activator-coactivator interactions in vivo. ACS Chem Biol 6, 1321–1326.
Kumagai PS, Martins CS, Sales EM, Rosa HVD, Mendonça DC, Damalio JCP, Spinozzi F, Itri R, Araujo APU (2019). Correct partner makes the difference: septin G-interface plays a critical role in amyloid formation. Int J Biol Macromol 133, 428–435.
Kuo Y-C, Lin Y-H, Chen H-I, Wang Y-Y, Chiou Y-W, Lin H-H, Pan H-A, Wu C-M, Su S-M, Hsu C-C, *et al*. (2012). SEPT12 mutations cause male infertility with defective sperm annulus. Hum Mutat 33, 710–719.
Laughery MF, Hunter T, Brown A, Hoopes J, Ostbye T, Shumaker T, Wyrick JJ (2015). New vectors for simple and streamlined CRISPR-Cas9 genome editing in Saccharomyces cerevisiae. Yeast 32, 711–720.
Lee K, Ziegelhoffer T, Delewski W, Berger SE, Sabat G, Craig EA (2021). Pathway of Hsp70 interactions at the ribosome. Nat Commun 12, 5666.
Lewis SA, Tian G, Cowan NJ (1997). The alpha- and beta-tubulin folding pathways. Trends Cell Biol 7, 479–484.
Li Z, Vizeacoumar FJ, Bahr S, Li J, Warringer J, Vizeacoumar FS, Min R, Vandersluis B, Bellay J, Devit M, *et al*. (2011). Systematic exploration of essential yeast gene function with temperature-sensitive mutants. Nat Biotechnol 29, 361–367.
Liu B, Han Y, Qian S-B (2013). Cotranslational response to proteotoxic stress by elongation pausing of ribosomes. Mol Cell 49, 453–463.
Lotz SK, Knighton LE, Nitika , Jones GW, Truman AW (2019). Not quite the SSAme: unique roles for the yeast cytosolic Hsp70s. Curr Genet 65, 1127–1134.
Lu J, Deutsch C (2008). Electrostatics in the ribosomal tunnel modulate chain elongation rates. J Mol Biol 384, 73–86.
Machida K, Miyawaki S, Kanzawa K, Hakushi T, Nakai T, Imataka H (2021). An in vitro reconstitution system defines the defective step in the biogenesis of mutated β-actin proteins. ACS Synth Biol 10, 3158–3166.
Makino Y, Amada K, Taguchi H, Yoshida M (1997). Chaperonin-mediated folding of green fluorescent protein. J Biol Chem 272, 12468–12474.
McMurray MA, Bertin A, Garcia G 3rd, Lam L, Nogales E, Thorner J (2011a). Septin filament formation is essential in budding yeast. Dev Cell 20, 540–549.
McMurray MA, Stefan CJ, Wemmer M, Odorizzi G, Emr SD, Thomer J (2011b). Genetic interactions with mutations affecting septin assembly reveal ESeRT functions in budding yeast cytokinesis. Biol Chem 392, 699–712.
McMurray MA, Thorner J (2008). Septin stability and recycling during dynamic structural transitions in cell division and development. Curr Biol 18, 1203–1208.
Mellacheruvu D, Wright Z, Couzens AL, Lambert J-P, St-Denis NA, Li T, Miteva YV, Hauri S, Sardiu ME, Low TY, *et al*. (2013). The CRAPome: a contaminant repository for affinity purification-mass spectrometry data. Nat Methods 10, 730–736.
Mendonça DC, Guimarães SL, Pereira HD, Pinto AA, de Farias MA, de Godoy AS, Araujo APU, van Heel M, Portugal RV, Garratt RC (2021). An atomic model for the human septin hexamer by cryo-EM. J Mol Biol 433, 167096.
Mendonça DC, Macedo JN, Guimarães SL, Barroso da Silva FL, Cassago A, Garratt RC, Portugal RV, Araujo APU (2019). A revised order of subunits in mammalian septin complexes. Cytoskeleton 76, 457–466.
Morán Luengo T, Mayer MP, Rüdiger SGD (2019). The Hsp70-Hsp90 chaperone cascade in protein folding. Trends Cell Biol 29, 164–177.
Naicker MC, Seul Jo I, Im H (2012). Identification of chaperones in freeze tolerance in Saccharomyces cerevisiae. J Microbiol 50, 882–887.
Nakamura Y, Gojobori T, Ikemura T (2000). Codon usage tabulated from international DNA sequence databases: status for the year 2000. Nucleic Acids Res 28, 292.
Nelson RJ, Ziegelhoffer T, Nicolet C, Werner-Washburne M, Craig EA (1992). The translation machinery and 70 kd heat shock protein cooperate in protein synthesis. Cell 71, 97–105.
Nissley DA, Jiang Y, Trovato F, Sitarik I, Narayan KB, To P, Xia Y, Fried SD, O'Brien EP (2022). Universal protein misfolding intermediates can bypass the proteostasis network and remain soluble and less functional. Nat Commun 13, 3081.
Nitika, Zheng B, Ruan L, Kline JT, Sikora J, Torres MT, Wang Y, Takakuwa JE, Huguet R, Klemm C, *et al*. (2021). A novel multifunctional role for Hsp70 in binding post-translational modifications on client proteins. BioRxiv 2021.08.25.457671.
Pan F, Malmberg RL, Momany M (2007). Analysis of septins across kingdoms reveals orthology and new motifs. BMC Evol Biol 7, 103.
Pavlov MY, Watts RE, Tan Z, Cornish VW, Ehrenberg M, Forster AC (2009). Slow peptide bond formation by proline and other N-alkylamino acids in translation. Proc Natl Acad Sci USA 106, 50–54.
Raval S, Sarpe V, Hepburn M, Crowder DA, Zhang T, Viner R, Schriemer DC (2021). Improving spectral validation rates in hydrogen-deuterium exchange data analysis. Anal Chem 93, 4246–4254.
Rey M, Sarpe V, Burns KM, Buse J, Baker CAH, van Dijk M, Wordeman L, Bonvin AMJJ, Schriemer DC (2014). Mass spec studio for integrative structural biology. Structure 22, 1538–1548.
Riba A, Di Nanni N, Mittal N, Arhné E, Schmidt A, Zavolan M (2019). Protein synthesis rates and ribosome occupancies reveal determinants of translation elongation rates. Proc Natl Acad Sci USA 116, 15023–15032.
Rivlin N, Katz S, Doody M, Sheffer M, Horesh S, Molchadsky A, Koifman G, Shetzer Y, Goldfinger N, Rotter V, *et al*. (2014). Rescue of embryonic stem cells from cellular transformation by proteomic stabilization of mutant p53 and conversion into WT conformation. Proc Natl Acad Sci USA 111, 7006–7011.
Robichon C, Luo J, Causey TB, Benner JS, Samuelson JC (2011). Engineering Escherichia coli BL21(DE3) derivative strains to minimize E. coli protein contamination after purification by immobilized metal affinity chromatography. Appl Environ Microbiol 77, 4634–4646.
Roggenkamp E, Giersch RM, Wedeman E, Eaton M, Turnquist E, Schrock MN, Alkotami L, Jirakittisonthon T, Schluter-Pascua SE, Bayne GH, *et al*. (2017). CRISPR-UnLOCK: multipurpose Cas9-based strategies for conversion of yeast libraries and strains. Front Microbiol 8, 1773.
Sambrook J, Russell DW (2006). Preparation and transformation of competent E. coli using calcium chloride. Cold Spring Harb Protoc 2006, pdb.prot3932.
Schaefer RM, Heasley LR, Odde DJ, McMurray MA (2016). Kinetic partitioning during de novo septin filament assembly creates a critical G1 "window of opportunity" for mutant septin function. Cell Cycle 15, 2441–2453.
Schindelin J, Arganda-Carreras I, Frise E, Kaynig V, Longair M, Pietzsch T, Preibisch S, Rueden C, Saalfeld S, Schmid B, *et al*. (2012). Fiji: an open-source platform for biological-image analysis. Nat Methods 9, 676–682.
Sen ND, Zhou F, Ingolia NT, Hinnebusch AG (2015). Genome-wide analysis of translational efficiency reveals distinct but overlapping functions of yeast DEAD-box RNA helicases Ded1 and eIF4A. Genome Res. 25, 1196–1205.
Shah R, Large AT, Ursinus A, Lin B, Gowrinathan P, Martin J, Lund PA (2016). Replacement of GroEL in Escherichia coli by the group II chaperonin from the archaeon Methanococcus maripaludis. J Bacteriol 198, 2692–2700.
Shalgi R, Hurt JA, Krykbaeva I, Taipale M, Lindquist S, Burge CB (2013). Widespread regulation of translation by elongation pausing in heat shock. Mol Cell 49, 439–452.
Sharma AK, Venezian J, Shiber A, Kramer G, Bukau B, O'Brien EP (2021). Combinations of slow-translating codon clusters can increase mRNA half-life in Saccharomyces cerevisiae. Proc Natl Acad Sci USA 118, e2026362118.
Shimizu Y, Inoue A, Tomari Y, Suzuki T, Yokogawa T, Nishikawa K, Ueda T (2001). Cell-free translation reconstituted with purified components. Nat Biotechnol 19, 751–755.
Shimon L, Hynes GM, McCormack EA, Willison KR, Horovitz A (2008). ATP-induced allostery in the eukaryotic chaperonin CCT is abolished by the mutation G345D in CCT4 that renders yeast temperature-sensitive for growth. J Mol Biol 377, 469–477.
Shuman B, Momany M (2021). Septins from protists to people. Front Cell Dev Biol 9, 824850.
Sirajuddin M, Farkasovsky M, Hauer F, Kühlmann D, Macara IG, Weyand M, Stark H, Wittinghofer A (2007). Structural insight into filament formation by mammalian septins. Nature 449, 311–315.
Sopko R, Huang D, Preston N, Chua G, Papp B, Kafadar K, Snyder M, Oliver SG, Cyert M, Hughes TR, *et al*. (2006). Mapping pathways and phenotypes by systematic gene overexpression. Mol Cell 21, 319–330.
Stein KC, Kriel A, Frydman J (2019). Nascent polypeptide domain topology and elongation rate direct the cotranslational hierarchy of Hsp70 and TRiC/CCT. Mol Cell 75, 1117–1130.e5.

Takagi J, Cho C, Duvalyan A, Yan Y, Halloran M, Hanson-Smith V, Thorner J, Finnigan GC (2021). Reconstructed evolutionary history of the yeast septins Cdc11 and Shs1. G3 (Bethesda) 11, jkaa006.
Tian G, Vainberg IE, Tap WD, Lewis SA, Cowan NJ (1995a). Specificity in chaperonin-mediated protein folding. Nature 375, 250–253.
Tian G, Vainberg IE, Tap WD, Lewis SA, Cowan NJ (1995b). Quasi-native chaperonin-bound intermediates in facilitated protein folding. J Biol Chem 270, 23910–23913.
Tong Z, Gao X-D, Howell AS, Bose I, Lew DJ, Bi E (2007). Adjacent positioning of cellular structures enabled by a Cdc42 GTPase-activating protein-mediated zone of inhibition. J Cell Biol 179, 1375–1384.
Ude S, Lassak J, Starosta AL, Kraxenberger T, Wilson DN, Jung K (2013). Translation elongation factor EF-P alleviates ribosome stalling at polyproline stretches. Science 339, 82–85.
Vainberg IE, Lewis SA, Rommelaere H, Ampe C, Vandekerckhove J, Klein HL, Cowan NJ (1998). Prefoldin, a chaperone that delivers unfolded proteins to cytosolic chaperonin. Cell 93, 863–873.
Van Durme J, Maurer-Stroh S, Gallardo R, Wilkinson H, Rousseau F, Schymkowitz J (2009). Accurate prediction of DnaK-peptide binding via homology modelling and experimental data. PLoS Comput Biol 5, e1000475.
Varadi M, Anyango S, Deshpande M, Nair S, Natassia C, Yordanova G, Yuan D, Stroe O, Wood G, Laydon A, *et al.* (2022). AlphaFold Protein Structure Database: massively expanding the structural coverage of protein-sequence space with high-accuracy models. Nucleic Acids Res. 50, D439–D444.
Versele M, Gullbrand B, Shulewitz MJ, Cid VJ, Bahmanyar S, Chen RE, Barth P, Alber T, Thorner J (2004). Protein-protein interactions governing septin heteropentamer assembly and septin filament organization in Saccharomyces cerevisiae. Mol Biol Cell 15, 4568–4583.
Versele M, Thorner J (2004). Septin collar formation in budding yeast requires GTP binding and direct phosphorylation by the PAK, Cla4. J Cell Biol 164, 701–715.
von Plehwe U, Berndt U, Conz C, Chiabudini M, Fitzke E, Sickmann A, Petersen A, Pfeifer D, Rospert S (2009). The Hsp70 homolog Ssb is essential for glucose sensing via the SNF1 kinase network. Genes Dev 23, 2102–2115.
Wang Q, Wang L (2008). New methods enabling efficient incorporation of unnatural amino acids in yeast. J Am Chem Soc 130, 6066–6067.
Wang Z, Feng HP, Landry SJ, Maxwell J, Gierasch LM (1999). Basis of substrate binding by the chaperonin GroEL. Biochemistry 38, 12537–12546.
Warnecke T, Hurst LD (2010). GroEL dependency affects codon usage—support for a critical role of misfolding in gene evolution. Mol Syst Biol 6, 340.
Weems AD, Johnson CR, Argueso JL, McMurray MA (2014). Higher-order septin assembly is driven by GTP-promoted conformational changes: evidence from unbiased mutational analysis in Saccharomyces cerevisiae. Genetics 196, 711–727.
Weems AD, McMurray MA (2017). The step-wise pathway of septin hetero-octamer assembly in budding yeast. eLife 6, e23689.
Weirich CS, Erzberger JP, Barral Y (2008). The septin family of GTPases: architecture and dynamics. Nat Rev Mol Cell Biol 9, 478–489.
Weissman JS, Rye HS, Fenton WA, Beechem JM, Horwich AL (1996). Characterization of the active intermediate of a GroEL-GroES-mediated protein folding reaction. Cell 84, 481–490.
Willmund F, del Alamo M, Pechmann S, Chen T, Albanèse V, Dammer EB, Peng J, Frydman J (2013). The cotranslational function of ribosome-associated Hsp70 in eukaryotic protein homeostasis. Cell 152, 196–209.
Winzeler EA, Shoemaker DD, Astromoff A, Liang H, Anderson K, Andre B, Bangham R, Benito R, Boeke JD, Bussey H, *et al.* (1999). Functional characterization of the S. cerevisiae genome by gene deletion and parallel analysis. Science 285, 901–906.
Wiśniewski JR (2016). Quantitative evaluation of filter aided sample preparation (FASP) and multienzyme digestion FASP protocols. Anal Chem 88, 5438–5443.
Woods BL, Gladfelter AS (2021). The state of the septin cytoskeleton from assembly to function. Curr Opin Cell Biol 68, 105–112.
Yam AY, Xia Y, Lin H-TJ, Burlingame A, Gerstein M, Frydman J (2008). Defining the TRiC/CCT interactome links chaperonin function to stabilization of newly made proteins with complex topologies. Nat Struct Mol Biol 15, 1255–1262.
Yan W, Schilke B, Pfund C, Walter W, Kim S, Craig EA (1998). Zuotin, a ribosome-associated DnaJ molecular chaperone. EMBO J 17, 4809–4817.
Ying B-W, Taguchi H, Ueda T (2006). Co-translational binding of GroEL to nascent polypeptides is followed by post-translational encapsulation by GroES to mediate protein folding. J Biol Chem 281, 21813–21819.
Yochem J, Uchida H, Sunshine M, Saito H, Georgopoulos CP, Feiss M (1978). Genetic analysis of two genes, dnaJ and dnaK, necessary for Escherichia coli and bacteriophage lambda DNA replication. Mol Gen Genet 164, 9–14.
Zhao L, Castanié-Cornet M-P, Kumar S, Genevaux P, Hayer-Hartl M, Hartl FU (2021). Bacterial RF3 senses chaperone function in co-translational folding. Mol Cell 81, 2914–2928.e7.
Zhu H, Bilgin M, Bangham R, Hall D, Casamayor A, Bertone P, Lan N, Jansen R, Bidlingmaier S, Houfek T, *et al.* (2001). Global analysis of protein activities using proteome chips. Science 293, 2101–2105.
Zuker M (2003). Mfold web server for nucleic acid folding and hybridization prediction. Nucleic Acids Res 31, 3406–3415.